Revision report and Author's response to the Reviewer comments

We thank to the reviewers who provided precise and valuable feedbacks on our manuscript. We addressed all the points in the responses as follows. We are happy to submit the revised manuscript that reflects these changes, which significantly improves the quality of our manuscript.

The reviewer comments are quoted in italic with some minor editorial adjustments, and our responses to them follows them. All the comments are numbered (A0, B002, etc), and corresponding changes in the text and figures are annotated on the margins in the revised manuscript. Some modification are separated into multiple blocks and each of them is annotated with the same tag. Those changes corresponding to Reviewer ♯1 and to ♯2 are marked with red and blue, respectively, which include deletion/addition/replacement of the figures. Since numbers of figures and equations are changed, there are many small changes in these reference numbers, which are annotated with brown tags in the revised manuscript. Also, after including all the changes, English check is done by a company, which is also annotated with brown.

Response to Anonymous Reviewer ♯1

We thank the reviewer for presenting several key points that will indeed improve the manuscript. We have addressed these concerns below.

Summary

(A0) ***F. Saito et al. paper addresses the problem of numerical computation of ice age in ice sheet models. Indeed, calculation of ice age is the major challenge of ice sheet modeling in various applications beginning with the preliminary choice of potential target place for deep drilling of ice sheets and ending with the accurate interpretation of ice cores. The study area in Saito et al. manuscript is limited by a summit position of an ice sheet where the benchmark — an analytical solution for the ice age can be set. The authors examine two semi-Lagrangian RCIP schemes performance and compare results with more traditional Eulerian upwinding schemes for solving an advection equation.***

Thank you very much for your summary. We agree that the topic of the manuscript is limited to 1-d computation under summits, and believe that this is a necessary step for future extension of the new scheme to 3-d field computation, as the referee remarks in the following.

General remarks

(A1) ***It should be noted that a family of RCIP schemes have been applied earlier in various problems of hydrodynamics, hydraulics etc., but their application for ice age calculation in ice sheet modeling is a novel and, perhaps, a promising approach. In reality, of course, we face with 3D problems of ice age computation, either when it is necessary to build the ice age field of the whole ice sheet or to construct a model chronology of a virtual ice core. From this point of view, the submitted research of***

Saito et al. may be considered as just an academic exercise comparing various numerical methods for highly idealized environmental conditions, which never occur in reality. Nevertheless, such kind of research are useful because they indicate possible pitfalls of rather traditional methods and introduce new approaches for solving tantalizing tasks in ice sheet modeling. In the 'Discussion and conclusion' section the authors reasonably point that the advection problem can be attributed not only to ice age calculation but also to calculation, for instance, of ice temperature. Anyway, further application of the RCIP method and its comparison with the Eulerian schemes in 3D will inevitably face with the choice of a true benchmark, which are, indeed, absent except in case of visual calculation of annual ice layers in ice cores. Moreover, for model interpretation of ice cores a very effective back-tracing method was suggested (Huybrechts et al., Climate of the Past, 2007) which is a powerful tool for dating of ice cores using ice sheet modeling technique. In the 'Discussion and conclusion' section authors mention that their aim is to proceed with examination of the RCIP scheme in 3D. In this view, I think it would be reasonable to outline possible restrictions, challenges and limitations of future research.

First of all, thank you for the evaluation and your precise understanding of this paper. Yes, this paper may be regarded as an exercise, however, as the reviewer kindly points out, we believe that this is a useful approach which we should not avoid when introducing a new scheme.

We agree in particular to the last remark. Citing Huybrechtes et al. (2007), we introduced possible restrictions and limitations of this approach in the discussion section. The small but main advantage of RCIP method than the powerful back-tracing method is that it is a forward scheme — it is not necessary to record all the past velocity field during the simulation. RCIP may do a good job for preserving the flux information at the deposition (annual layer thickness in the case of dating), however, detection of 'points of origin' requires another technique, e.g., the back-tracing method itself. Thus we consider that the combination of the high precision forward scheme and the powerful backward scheme will be a good choice for ice-core dating issue. Thanks a lot for this comment.

(A2) ***Another problem, which was not elucidated in the manuscript is the computational cost of application of different numerical schemes. I think it would be easy to do since all experiments were performed on the same computer facility. There is only short note on that (Line 239). The trade off between time of computation and accuracy in some cases may play for the simpler but faster method. In general, the manuscript is well structured, the figures are informative (except the note below concerning an a possible additional figure).***

Thanks a lot for pointing it out. Typically we computed 4×7 different configuration of 1d column in one run on an Intel Xeon E5-2609 6 core PC. The mean computational costs for one job in the case of 129 levels with the first-order upstream, the second-order, RCIP, RCIP with correction are 30, 28, 32, and 34 seconds, respectively. Those in the case of 513 levels are 338, 296, 364 and 392 seconds, respectively. These are described in the text in addition to the original text relating to the ratio of computing times.

Line by line comments

(A000) ***The title of the paper. The core of the paper is a set of comparisons between performance of the semi-Lagrangian RCIP schemes and the Eulerian once. Actually, there is nothing in the manuscript about ice sheet models. Therefore, it would be reasonable to be more precise in formulation of the title.***

Thanks a lot for your suggestion. In particular for title, we agree to your suggestion. Since the word 'ice-sheet' should be kept because the focus is on it, only the last word is not necessary to satisfy your remark — 'Implementation of RCIP scheme and its performance for 1D age computations in ice-sheet'. Generally, however, 'an ice-sheet model' means various things: recently in most context it seems a dynamic ice-sheet *flow* model, but an ice-sheet *dating* model can be also an ice-sheet model. Also, as discussed shortly in the manuscript, we will extend RCIP implementation onto our ice-sheet *flow* model, so we keep most of the terminology in the main text.

(A001) ***Line 15. "$\cdots$ more generally in tracer transport $\cdots$". This statement is somewhat confusing. Dating of ice cores is not limited to tracer transport. This definition (tracer transport) may be attributed to Lagrangian or semi-Lagrangian methods only.***

All right, we agree it was confusing. The block 'tracer transport...' are now deleted. Also the paragraph are slightly adjusted according to this change.

(A002) ***Section 1.1 and 1.2 The section lacks short general description of the semi-Lagrangian method in the context of its comparison with the pure Lagrangian and the Eulerian. Since the problem of interpolation is the most important in semi-Lagrangian schemes, it will be very much handful to make a (sketch) figure illustrating application of a 1-D semi-Lagrangian approach using definitions of the variables mentioned in the manuscript (arrival and departure points etc.). It would be also appropriate to address the reader to a classical paper (Stanoforth and Côté, 1991, Semi-Lagrangian integration schemes for atmospheric models: a review. Mon.Weather Rev., 119(9), 2206-2223.)***

This is a good point. A short general descriptions are inserted in Sects 1.1 and 1.2 with a schematic figure to explain the design of semi-Lagrangian, arrival/departure points (new Figure 1). The classical paper the reviewer mentioned is cited also.

(A003) ***Line 61. Please comment on the first use of $g(x_j)$. What is it, what is the purpose of its introduction etc.***

The term $g(x_j)$ is abbreviation of function $g(x)$ (i.e. the spatial derivative of $f(x)$) at the grid-points x_j. The definition of $g(x)$ was already documented before Eq.(4), but A short description is inserted again here in order to emphasize it.

(A004) ***Line 187. To be precise, Rybak and Huybrechts (2003) did not employ semi-Lagrangian approach, but pure Lagrangian particle tracing.***

Thanks. 'Lagrangian' is also inserted here.

(A005) ***Line 394. "Figure 14 is the result$\cdots$" should be reformulated like, for instance, "Results of transient experiments are presented in Figure 14 $\cdots$". Same is in Line 395: "same as IN Fig. 6 AND 7." Same is in the next sentence.***

They are reformulated following your suggestions, with including the suggestion of the reviewer ii.

(A006) ***Line 459. Please, check equation for ζ. What is Z^{14}? Please, explain why did you use this particular formula for the smooth discretization? What did you mean under "some trial and error". In my view, you should be more exact.***

Thanks a lot for point it out. The term Z^{14} is Z to the power of 14. We try the ζ formulation as $(Z + \gamma Z^{\psi})/(1 + \gamma)$ with two parameters γ and ψ. The constrain we force was (i) $\zeta(Z = 0) = 0$ (ii) $\zeta(Z = 1) = 1$, (iii) $d\zeta/dZ > 0$. The formulation above is simple and satisfy these requirements. With varying x and y, we found the formulation in the text is one of them to resolve the target annual layer thickness at the target depth. These are now described around here.

(A007) ***Line 482. Please, indicate that your computations can be related to the summit points of ice sheets only, which are accepted stable throughout the time spell of numerical experiments.***

All right. The restriction of this study as you mention is now inserted.

(A008) ***Line 482. In my view, the fragment of the text "$\cdots$ ice-sheets under various configurations" is somewhat confusing. The results of the study are attributed to summits of ice sheets only, and their configurations have no any connection with the research.***

All right. The word 'various' is too much and removed. Together with the previous remark, the sentence are written more precisely. Thanks a lot.

Response to Reviewer ♯2

We thank Shawn Marshall for a number of detailed review that significantly helped us to improve the quality of our manuscript. We have addressed these concerns below.

(B0) ***The authors present a detailed examination of a novel (in ice sheets) interpolation scheme with promise for improved tracing of ice age as well as annual layer thickness reconstructions in ice sheets. This study focuses on 1D examples with scenarios (e.g. mass balance accumulation rates/vertical velocities) typical of the East Antarctic plateau, with direct relevance to ice core dating and age modelling.***

Thank you very much for your summary.

(B1) ***The study is comprehensive, with superb attention to detail and to explaining the method and the mathematical implementation, such that this should provide a strong foundation for building on and for others that choose to adopt these methods. It is a valuable study, as age modelling or other passive tracer advection studies (e.g., isotopes, dust layers, or other chemical horizons) have not been given much attention in ice sheet studies in recent years, and are likely due for a resurgence as radar reconstructions are giving increasing detail on 3D ice sheet structure (e.g. McGregor et al., 2015); 3D tracer modelling offers an important avenue for improving and constraining ice sheet models. The methods introduced here should be seriously considered as an alternative to more 'classical' semi-Lagrangian interpolation schemes such as upwind differencing.***
MacGregor, J. A., M. A. Fahnestock, G. A. Catania, J. D. Paden, S. Prasad Gogineni, S. K. Young, S. C. Rybarski, A. N. Mabrey, B. M. Wagman, and M. Morlighem (2015a), Radiostratigraphy and age structure of the Greenland Ice Sheet, J. Geophys. Res. Earth Surf., 120, 212–241, doi:10.1002/2014JF003215.

Thanks a lot for such a positive evaluation.

(B2) ***I am attaching a copy of the manuscript with several minor points. The English needs a bit of a double check throughout, for articles, but it is extremely well written and thorough, overall. I will confess that I did not work through the mathematical derivations carefully and have no experience with the RCIP or CIP techniques, so I cannot comment specifically on the rigour and appropriateness of this aspect of the manuscript, or on the novelty of the ideas (vs. e.g., existing implementations in other contexts such as atmospheric models). It is new and relevant to ice sheet modelling.***

Responses to all the minor points are appended at the next section. We are grateful to the reviewer for the careful and detail review. We believe that the manuscript is now significantly improved after modification following the suggestions and comments.

(B3) ***There is a large number of figures, and it could be worthwhile to consider condensing the presentation of results a little. For instance, with new experiments/sensitivity tests after Figure 7, it could be possible to show only one result (of Figures 8 and 9, and of Figures 14 and 15; maybe elsewhere), while still***

discussing both experiments in the text. I am also OK with the manuscript as is. Sometimes it is nice to see everything laid out and presented, without relegating additional results to supplements.

All right, we agree. We reduce the figures while keeping the text accordingly. Figures 9, 13, 15 are now removed.

(B4) ***A couple of suggestions for the authors' consideration:***
The accumulation rates in the experiments are very low, typical of the East Antarctic Plateau during the glacial period. I guess that it does not affect the performance of the different interpolation/advection models, but am curious to confirm this for the case of e.g. accumulation rates 10 times higher, more typical of Greenland. Also, combined with this, high-amplitude, millennial-scale climate oscillations that are typical of Greenland (D-O cycles). Are there specific recommendations or differences in RCIP behaviour specific to these conditions?

This is a good point.

Actually, as far as the shapes of normalized vertical velocity profile are identical, the normalized shapes of the solutions are also identical. In other words, for example, the age solution under the configuration of 30cm/yr surface mass balance, 0 basal mass balance, and 3000m ice thickness, has the same normalized shape with the solution with that under 3cm/yr, 0 and 3000m, respectively. Another example: Fig. 17 in the manuscript shows the results of annual layer thickness at **1000kyr** in terms of **mm**, under the square wave surface mass balance between **3cm/yr** and **1.5cm/yr** with total duration of **10**,**20**, and **50kyr**. These results can be, as they are, interpreted as annual layer thickness at **100kyr** in terms of **10mm**, under those of **30cm/yr**–**15cm/yr** with the duration **1**, **2**, and **5kyr**, respectively (i.e., corresponding 1/10 unit time.). Therefore roughly speaking, the situation the referee is interested (millennial scale and typical Greenland) is already covered by the same experiment. We have examined a part of sensitivity studies with 10 times higher accumulation to confirm the above idea (figure is not shown). The idea of scaling can be additional demonstration worthwhile to present. We insert this idea in the introduction and result section, and also insert actual discussion in the last section. Thanks a lot for this point.

(B5) ***The model is developed specific to 1D age modelling in ice core settings (i.e. purely vertical flow, positive surface mass balance). Extension to 3D is discussed near the end, but would require consideration of positive (emergence) velocities, 3D flow fields, and (typically) much lower horizontal gradients of ice age. This first comes up on p.8, l.197, where the authors develop a formulation that assumes negative vertical velocity throughout, which will not be compatible with 3D modelling. I appreciate that the extension to 3D is for future study and we already have much to chew on with the current presentation of ideas and results, but this discussion could be extended a bit and I am curious about the author's opinion of whether the more complex RCIP type of approach is warranted for the lower horizontal gradients in 3D interpolation models.***

Yes, the negative mass balance experiment is just a demonstration and may not be compatible with 3d situation. RCIP is in a sense merely a variation of semi-Lagrangian scheme: instead of

spatially increasing the number of grid-points for achieve higher-order interpolation, it does add a field variable to solve (the gradient term). Therefore RCIP is essentially the same method with the other higher-order semi-Lagrangian scheme, so we believe that this approach has a comparable characteristics with other semi-Lagrangian schemes that the many past studies have already presented and discussed. In addition, the spatial gradient of age is not a diagnostic (passive) field but prognostic under the RCIP scheme. So we speculate that the precision of the spatial gradient is no worse (hopefully better) than the other higher-order semi-Lagrangian methods. Such an extension of this discussion are inserted in the text. Thanks a lot for such a stimulating comment to improve our manuscript.

(B6) ***Related to 3D models: the authors explore what would be considered as high vertical resolution in ice sheet models, from 129 to 513 vertical layers. This is much higher than many operational 3D ice sheet models that look at 3d (Stokes) solutions to the velocity field or Ice Age timescales: nz = 40 may be more typical. In the section on vertical resolution, it would be helpful to include an experiment with e.g. nz=33 to evaluation model performance at lower resolution. Does it further degrade the interpolation schemes and exaggerate the differences in modelled ice age, or do models converge as resolution declines?***

Actually, we have already performed, some of e.g., nz=33 cases. An example result is inserted in the manuscript (new Figure 17). Also, Fig. 14 (which was Fig.16 in the first manuscript) now contains a lines corresponding to nz=33. The preservation of annual layer thickness is reduced at shallower depth.

(B7) ***I am interested in the relatively strong results of the first-order upwind scheme. The authors do discuss this, but why is this consistently better than 2nd-order upwind schemes in almost all of the model experiments? In some cases it is of comparable performance to RCIP. Would the authors recommend always using 1st-order over 2nd-order upstream advection/interpolation models, and under what conditions might 1st-order advection schemes be adequate, vs. the RCIP-corr approach? A short discussion of 'practical suggestions' for eventual application of this technique in ice sheet models would be valuable.***

Yes, we were surprised to see that, too. The relatively better performance of the first-order upwind scheme is already presented in past studies (Greve et al 2002 cited at L282), which attributes to cancellation of errors between discretization and numerical diffusion. Moreover, as discussed in the manuscript, the design of mid-point rule on the first-order upwind scheme is not a *true* first-order scheme. Figure 3 presents that the solution by true first-order scheme (UP-1n) is worse by magnitude one than the second-order (UP-2), as we expected. It is possible to implement similar mid-point rule on the second-order scheme, which may improve the result of second-order Or, a different design of second-order scheme as Greve et al (2002). These may change the relative performances. Despite several difference of the past study, the result show similar performances qualitatively: the first-order results may better than the second-order except for the bottom.

Figure 3 also RCIP with upstream correction significantly improves the solution than RCIP without correction, which suggests an importance of non-constant velocity between the arrival and departure points to take into account. A mid-point rule formulation on the first-order scheme, in principle, corresponds to the former, with upstream correction.

The shape of normalized vertical velocity profile also may play a role for the relative performance. The bottom part is less *linear* than the upper part, thus the first-order approximation becomes worse. Some or all of these points lead the better performance of the first-order. We extend these discussion in the manuscript.

About practical suggestions. We considered that, as far as the annually layer thickness is not our concern, the classical upwind schemes are not a bad choice for dating. Using a first-order upwind scheme, a detail structure of surface mass balance history disappears very rapidly, but average features are quite well computed except for near the bottom. The second-order scheme preserves the history than the first, but without an effective slope limiter strange oscillation can strike the result as we demonstrated in the paper. We did not try any of such slope filters presented in the past studies because it is not our purpose, that is one of the reasons that second-order seems to be worse than the first. However, as far as the annually layer thickness is not a focus, the results by the second-order schemes are slightly better than those of the first-order throughout the experiment except for the most simple case (honestly, not better but more close to RCIP solution). Slope filters for higher-order upwind schemes on a non-uniform discretization is possible (as mentioned in the text citing Murman et al 2005), but rather complex than uniform discretization case. The conclusion of Greve et al (2002) already present such 'practical suggestions': the second-order, the TVDLF scheme with minmod filter, and even the first-order schemes are their proposal for dating. Our suggestion after this statement: if you expect good performance in annual layer thickness computation close to the bottom, using non-uniform discretization, then we strongly recommends to apply RCIP. We cite their statement and our new suggestion are inserted accordingly. Thanks a lot for pointing it out.

(B8) ***Many thanks for this interesting contribution - I look forward to seeing the final version advance to GMD and push the research community forward.***

Again, thanks a lot for all of the fruitful comments which definitely improve out manuscripts.

Minor points

(B000) ***page=1 areas. Or "the potential ... area."***

All right. Replaced with 'areas'.

(B001) ***page=2 I feel compelled to note that this work on semi-Lagrangian tracer schemes was initiated in Clarke and Marshall (2002), and Tarasov and Peltier (2003) built off of this. Clarke et al. (2005) and Lhomme et al. (2005) built further, through the introduction of mass-balance based interpolation schemes to better address the age-depth relationship (as noted here) in several different Greenland cores. Clarke, G.K.C., Marshall, S.J., 2002. Isotopic balance of the Greenland Ice Sheet: modelled concentrations of water isotopes from 30,000 BP to present. Quaternary Science Reviews 21, 419–430***

Good point. Thank you very much for the information. We introduce Clark and Marshall (2005) here and other places.

(B002) ***page=2 performing a time-splitting....***

All right, inserted 'a', accordingly.

(B003) ***page=2 on the time-splitting...***

All right, inserted 'the', accordingly.

(B004) ***page=5 here, does x refer to x_{dep}, per the line above? Or it would be more logical to me that x_j in Eq (24) is x_{dep}, the fixed point of departure.***

After posting of the author's comment, we found an error on Eq. (24), which may confuse the reviewer. The function of Eq. (24) is a linear formulation of u on any x between x_j and x_{jj+1}, not between x_j and x_{jj+1} as in the original submission. So, any x between x_j and x_{jj+1}, including $x = x_{dep}$ satisfies this formulation, as the reviewer pointed out. In order to integrate along x between x_j and x_{dep}, we need such a formulation for x in this range. Correcting the error, we believe that this point is more clearly described now. We are sorry about the mistake, and thanks a lot to the reviewer for pointing it out.

(B005) ***page=6 delete "of"***

All right, deleted 'of' accordingly.

(B006) ***page=7 Do you mean Eq. (32) here?***

Correct. Thanks a lot.

(B007) ***page=7 is adopted***

Thanks a lot. We modified the noun (representations) instead.

(B008) ***page=8 Clarke and Marshall, 2002***

Thanks a lot. Together with citation of the paper at page 2, this is introduced.

(B009) ***page=8 although note that this will fail to accommodate full ice sheet conditions, e.g. in tracing layers into ablation zones***

You are right. This sentence somewhat overstates ice sheet dating computation. We modify the statement according to your comment.

(B010) ***page=10 computations***

All right, 'computations' accordingly.

(B011) ***page=10 what do you mean, for p? for p=1?***

Sorry, the correct sentence is '... and setting $Ms = -Mb$ for arbitrarily p.' The word 'arbitrarily' was placed at wrong position.

(B012) ***page=10 suggest $\sim$ rather than "around", here and later in this sentence***

All right. 'Around' hear and later are be replaced with '$\sim$'.

(B013) ***page=12 We use a...***

All right. Rewritten as 'We use a uniform grid spacing of ...' accordingly.

(B014) ***page=12 I am unclear on the units here - this is the error in years, perhaps, rather than kyr? At face values, it appears to have negative and positive biases of more than 10 kyr, but that is not consistent with (a)***

The unit is correct. Indeed the small oscillation at the bottom in (b) is obscured by the benchmark line in (a). Zooming up of the figure (c) is inserted.

(B015) ***page=13 as a vertical***

All right, inserted 'a', accordingly.

(B016) ***page=13 a very simple***

All right, inserted 'a', accordingly.

(B017) ***page=14 These values are all fine but are extremely low for a lot of glaciological situations, e.g. in Greenland or WAIS divide, etc. Perhaps reflective of the glacial Antarctica plateau (3 cm/yr), but sensitivity tests could explore values and order of magnitude higher than this to be more representative of other ice sheet conditions.***

We definitely agree to this point. Please check our response above (B4). Roughly speaking, the proper scaling of the result are examined. Also, the additional experiments with 10-times larger accumulation are discussed here, which may draw more attention from readers. Thanks a lot for the suggestion.

(B018) ***page=15 Did you explore sensitivity to nz? It might be good to discuss - nz=129 is greater resolution than many ice sheet modelling studies.***

Actually, yes (see response to B6). Using lower resolution, the preservation of annual layer thickness is reduced at shallower depth. This is discussed in the text.

(B019) ***page=20 of numerical performance of different schemes***

Thanks a lot. Corrected accordingly, with inserting a word 'levels'.

(B020) ***page=23 (a) to (c) are backwards here, I think***

Yes, that's right. Corrected accordingly. The labels above the figures are correct.

(B021) ***page=24 This is a great plot, but is hard to compare with the reference resolution in Figure 17 - perhaps each could be shown on the same y axis from e.g. 1000 to 2600 m?***

Great idea. We extend the y-axis accordingly. Thanks a lot.

(B022) ***page=25 a non-smooth grid***

All right. inserted 'a', accordingly.

Implementation of RCIP scheme and its performance for 1D age computations in ice-sheet ~~models~~

A000

Fuyuki SAITO[1], Takashi OBASE[2], and Ayako ABE-OUCHI[2,1]

[1]Japan Agency for Marine-Earth Science and Technology (JAMSTEC), Yokohama, Japan
[2]Atmosphere Ocean Research Institute, University ~~Univ.~~ of Tokyo, Kashiwa, Japan

Correspondence: SAITO Fuyuki (saitofuyuki@jamstec.go.jp)

Abstract. Ice sheet age computations are formulated using an Eulerian advection equation, and there are many schemes that can be used to solve them numerically. Typically, these differ in numerical characteristics such as stability, accuracy, and diffusivity. Furthermore, although various methods have been presented for ice sheet age computations, the constrained interpolation profile method and its variants have not been examined in this context. The present study introduces one of its variants, a rational function-based constrained interpolation profile scheme (RCIP) to one-dimensional ice age computation~~,~~ and demonstrates its performance levels via comparisons with those obtained from first- and second-order upwind schemes. Our results show that the RCIP scheme preserves the pattern of input surface mass balance histories~~,~~ in terms of the vertical profile of internal annual layer thickness, better than the other schemes.

1 Introduction

Core samples extracted from ice sheets can provide an archive of past climate history data, and a major issue for researchers attempting to utilize ice-core properties is defining the age of ice along the depth of the ice sheet. This process is often called *dating*. Dating with numerical ice-flow models is an important approach~~,~~ because it allows researchers to~~one can~~ estimate age profiles before actual drilling of ice cores. For example, in Fischer et al. (2013), the authors present an application of ice-flow models to evaluate potential 'Oldest-Ice' study areas~~area~~.

B000

Various methods for use in ice-sheet model dating~~, or more generally in tracer transport~~ have been adopted and compared. Müggе et al. (1999) compared particle tracking (Lagrangian) and Eulerian schemes under simulated steady-state three-dimensional (3D) velocity fields of Antarctic ice sheet. That study concluded that the Eulerian scheme works well, except for the bottom part, which encounters problems due to numerical diffusion. In Rybak and Huybrechts (2003), the authors also compared the Lagrangian and Eulerian schemes for simulated Antarctic ice sheets under various schematic steady-state conditions and analytical solutions, as well as under different 3D velocity fields. Similarly, they concluded that the Lagrangian method produced less error than an Euler approach, although the difference was small over a large part of the domain. Greve et al. (2002) compared several Eulerian schemes such as central difference schemes, first- and second-order upwind schemes, Quadratic Upstream Interpolation for Convective Kinematics (QUICK), and total variation diminished (TVD) Lax-Wendroff (LW) schemes. From comparisons of the one-dimensional (1D) steady-state age profiles produced by these schemes, they

A001

concluded that the second-order upwind and TVD-LW schemes performed well for typical ice sheet age profiles. Comparisons among semi-Lagrangian schemes have also been performed. Introduction of a semi-Lagrangian trace scheme to ice-sheet modeling was initiated by Clarke and Marshall (2002). They simulate the temporal and spatial variations of water isotopes in the Greenland Ice Sheet over the past 30,000 years. In Tarasov and Peltier (2003), the authors compared various interpolation schemes in order to compute upwind departure points in a semi-Lagrangian tracer model in terms of preservation of input signal phases and amplitudes, while Lhomme et al. (2005); Clarke et al. (2005) developed a new interpolation method that can be used in a semi-Lagrangian scheme, and discussed computed ice-core age-depth relationships for the Greenland Ice Core Project (GRIP) ice-core.

To date, various methods have been presented and demonstrated for use in ice-sheet age computations. However, there are still a variety of numerical schemes that have not been examined within this context. These include the constrained interpolation profile (CIP) method (e.g., Yabe et al., 2001) and its variants. Accordingly, the present study introduces a CIP method variant named the rational function-based constrained interpolation profile (RCIP) method (Xiao et al., 1996) for use in 1D ice age computations and demonstrates the performance of the scheme.

1.1 Brief introduction of RCIP scheme

This section describes a standard algorithm of the CIP scheme family that is used to solve a 1D advection equation with a non-advection term as follows:

$$\frac{\partial f}{\partial t} + u(x,t)\frac{\partial f}{\partial x} = h(x,t)\,, \tag{1}$$

where $f = f(x,t)$ is a free variable to solve, $u = u(x,t)$ is a velocity field, $h = h(x,t)$ is an arbitrarily (non-advection) field, and t and x are temporal and spatial coordinates, respectively.

As introduced in the previous section, there are three major approaches to solving an advection equation: Eulerian, Lagrangian, and semi-Lagrangian. The CIP scheme family corresponds to a semi-Lagrangian method variation. The basics of the semi-Lagrangian approach, within the context of its comparison with the Lagrangian and Eulerian approaches, have already been presented in a number of past studies. For example, Staniforth and Côté (1990) presented a review of these methods and described the implementation and application of a semi-Lagrangian method in detail. Although a full description of the semi-Lagrangian is not repeated in this paper, its basic principles will be described later in this section.

In CIP schemes, Eq. (1) is solved by performing a time-splitting algorithm (e.g., Yabe and Takei, 1988) into two phases as follows:

$$\frac{\partial f}{\partial t} + u(x,t)\frac{\partial f}{\partial x} = 0\,, \qquad \text{the advection phase} \tag{2}$$

$$\frac{\partial f}{\partial t} = h(x,t)\,. \qquad \text{the non-advection phase} \tag{3}$$

Appendix A presents a note on the time-splitting technique.

The primary characteristic of this CIP scheme is the introduction of an additional equation to solve the spatial derivatives of f at the same time. Differentiation of Eq. (1) provides the equation for $g(x,t) = \frac{\partial f}{\partial x}$:

$$\frac{\partial g}{\partial t} + u(x,t)\frac{\partial g}{\partial x} = \hat{h}(x,t) = \frac{\partial h}{\partial x} - g\frac{\partial u}{\partial x} \,. \tag{4}$$

Equation (4) is an advection formula that is similar to Eq. (1) with the non-advection function $\hat{h}(x,t)$ in the right-hand side, which is solved using a time-splitting procedure similar to those used in Eqs. (2) and (3):

$$\frac{\partial g}{\partial t} + u(x,t)\frac{\partial g}{\partial x} = 0 \,, \qquad \text{advection phase} \tag{5}$$

$$\frac{\partial g}{\partial t} = \hat{h}(x,t) \,. \qquad \text{non-advection phase} \tag{6}$$

The algorithm used to solve the advection phases (Eqs. 2 and 5), which is a core characteristic of the CIP scheme family, is described here, after which the algorithm~~followed by that~~ used to solve the non-advection phases (Eqs. 3 and 6) will be discussed.

In semi-Lagrangian approaches, a particle at $(x, t+\Delta t)$ originates from the position of the upstream departure point $x_{\rm dep}$ such that

$$f(x,t+\Delta t) = f(x_{\rm dep},t) \,, \tag{7}$$

where

$$x_{\rm dep} = x + \int_{t+\Delta t}^{t} {\rm d}t\, u(x,t) \,. \tag{8}$$

Figure 1 shows a schematic illustration of semi-Lagrangian scheme. The particle at x_j at time $t_m+\Delta t$ originates from a particle at $x_{\rm dep}$, which is not necessarily on a discretized grid point x_j. Therefore, the free variable $f(x)$ must be interpolated using the value on the grid points (represented by color shading in the figure). A002

The CIP method constructs an interpolation function $F_j(x)$ for the $f(x)$ between two adjacent grid-points x_j and its upwind point x_{j+1} when $u_j < 0$ in order to assess the value at the departure point. Introducing $\langle\xi\rangle = x_{\rm dep} - x_j$~~,~~ as the distance to the original point~~,~~ allows the time evolution of $f(x_j)$ (which is the original free variable to solve) and $g(x_j)$ (which is the spatial derivative of f at the grid-points x_j) to be solved as simple advection equations: A003 A003

$$\begin{cases} f(x_j,t+\Delta t) = f(x_j+\langle\xi\rangle,t) = F_j(x_j+\langle\xi\rangle) \,, \\ g(x_j,t+\Delta t) = g(x_j+\langle\xi\rangle,t) = G_j(x_j+\langle\xi\rangle) \,, \end{cases} \tag{9}$$

where $G_j(x) = \frac{\partial F_j}{\partial x}$. Note that computation~~Computation~~ of ~~the~~ distance to the departure point will be described in Sect. 1.2. The piecewise interpolation function $F_j(x)$ for $x_j \le x \le x_{j+1}$ is defined to be constrained by the continuity condition at x_j and x_{j+1} as

$$\begin{cases} F_j(x_j) = f(x_j), \quad F_j(x_{j+1}) = f(x_{j+1}), \\ G_j(x_j) = g(x_j), \quad G_j(x_{j+1}) = g(x_{j+1}). \end{cases} \tag{10}$$

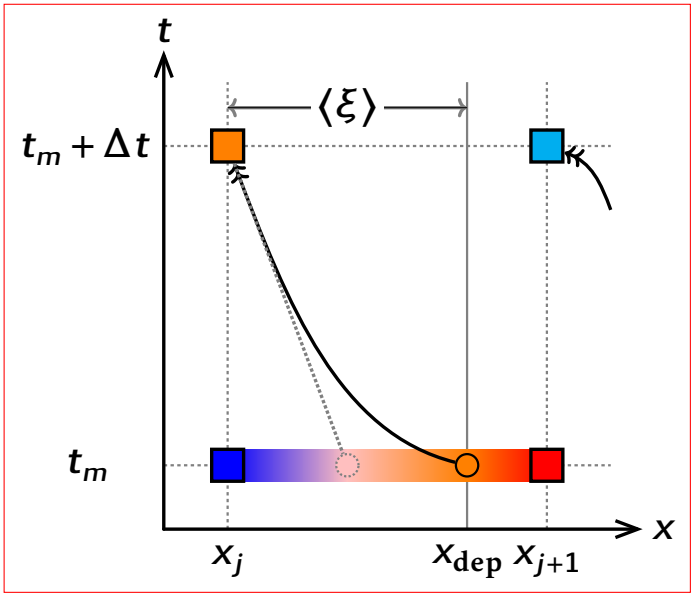

Figure 1. Schematic illustration of advection and semi-Lagrangian scheme. The new state computation for a target point x_j from time t_m in the case of $u_j < 0$ is presented. The colors symbolically express the value of field variables. The boxes correspond to model grid points. The solid arrow is the trajectory of one particle and the solid circle is the departure point. In a semi-Lagrangian scheme, the distance to the departure point, $\langle\xi\rangle$, is computed using an assumed trajectory. Interpolating the state at departure point $x_{\rm dep}$, the value is advected to the arrival point $(x_j, t_m + \Delta t)$. The dotted arrow and circle correspond to the trajectory and departure point in a different case while assuming a constant velocity, which may lead to a different state. A002

A cubic polynomial is chosen in the original CIP scheme, as

$$F_j(X) = C_0 + C_1 X + C_2 X^2 + C_3 X^3 \,, \tag{11}$$

where $X = x - x_j$. The four coefficients C_0, C_1, C_2, and C_3 in Eq. (11) are determined to satisfy the constraints (Eq. 10). The RCIP scheme framework is occasionally extended to introduce a rational function (Xiao et al., 1996) such as

$$F_j(X) = \frac{C_0 + C_1 X + C_2 X^2}{1 + D_1 X} \,. \tag{12}$$

The interpolation function is switched from the cubic (11) to the rational (12) if $g_j \le S_j \le g_{j+1}$ or if $g_j \ge S_j \ge g_{j+1}$, where

$$S_j = \frac{f_{j+1} - f_j}{\Delta x_{j+\frac{1}{2}}} \,, \qquad \Delta x_{j+\frac{1}{2}} = x_{j+1} - x_j \,. \tag{13}$$

Additionally, the four coefficients C_0, C_1, C_2, and D_1 are determined in order to satisfy the same constraints. The two interpolation functions Eqs. (11) and (12) are integrated by introducing a switching parameter α:

$$F_j(X) = \frac{C_0 + C_1 X + C_2 X^2 + C_3 X^3}{1 + \alpha D_1 X} \,. \tag{14}$$

The five coefficients used to satisfy the constraints are computed as

$$D_1 = \frac{1}{\Delta x_{j+\frac{1}{2}}} \left[\left| \frac{S_j - g_j}{g_{j+1} - S_j} \right| - 1 \right] , \tag{15}$$

$$C_3 = \frac{g_j - S_j + (g_{j+1} - S_j)(1 + \alpha D_1 \Delta x_{j+\frac{1}{2}})}{{\Delta x_{j+\frac{1}{2}}}^2} , \tag{16}$$

$$C_2 = S_j \alpha D_1 + \frac{S_j - g_j}{\Delta x_{j+\frac{1}{2}}} - C_3 \Delta x_{j+\frac{1}{2}} , \tag{17}$$

$$C_1 = g_j + f_j \alpha D_1 , \tag{18}$$

$$C_0 = f_j . \tag{19}$$

The switching parameter $\alpha \in [0, 1]$ is chosen as 1 when it is necessary to use rational interpolation. In other cases, 0 is selected. If $\{f_j\}$ and $\{g_j\}$ at time t are known, the new states $\{f_j^*\}$ and $\{g_j^*\}$ are predicted by shifting by distance along the characteristics (Eq. 9) to the departure point $\langle \xi \rangle$, as follows:

$$\begin{cases} f_j^* = F_j(\langle \xi \rangle) = \dfrac{C_0 + C_1 \langle \xi \rangle + C_2 \langle \xi \rangle^2 + C_3 \langle \xi \rangle^3}{1 + \alpha D_1 \langle \xi \rangle} , \\ g_j^* = G_j(\langle \xi \rangle) = \dfrac{C_1 + 2C_2 \langle \xi \rangle + 3C_3 \langle \xi \rangle^2}{1 + \alpha D_1 \langle \xi \rangle} - \dfrac{\alpha D_1}{1 + \alpha D_1 \langle \xi \rangle} f_j^* . \end{cases} \tag{20}$$

The solutions above are those of the advection phases (Eqs. 2 and 5). The time evolutions of f and g in the non-advection phases are again calculated according to Eqs. (3) and (6), typically by using a forwarding scheme, starting from the solution of the advection phase $\{f_j^*\}$ and $\{g_j^*\}$, as an intermediate solution:

$$\begin{cases} \dfrac{f_j(t + \Delta t) - f_j^*}{\Delta t} = h_j \\ \dfrac{g_j(t + \Delta t) - g_j^*}{\Delta t} = \hat{h}_j . \end{cases} \tag{21}$$

As discussed in Xiao et al. (1996), the formulation of the RCIP scheme possesses attractive properties, such as convexity and monotone preservation, as well as phase speed.

1.2 Upstream departure point

The interpolation method used for the field variables, which characterize each scheme, is one of the most important topics in semi-Lagrangian schemes. Another major topic common to the semi-Lagrangian schemes is the method used to compute the departure point.

A002

Equation (8) gives the distance to the departure point:

$$\langle \xi \rangle = - \int_t^{t+\Delta t} \mathrm{d}t \, u(x, t) . \tag{22}$$

A simple and primitive way to integrate Eq. (22) is to use the local velocity even if the velocity is a function of time and space (e.g., Toda et al., 2009), such that

$$\langle \xi \rangle = -u_j \Delta t \,. \tag{23}$$

Figure 1 shows a trajectory and departure point under a constant velocity (dotted line and circle) assumption. As can be seen, the computed departure point can be different from a general non-uniform velocity situation. Another way is to apply the 'mid-point rule', where both spatial and temporal mean velocity between the target and departure points replaces u_j in Eq. (23), which is generally computed in an iterative fashion (Tarasov and Peltier, 2003). In the present paper, a third approach is adopted. First, a steady and linear velocity field between the target and the upstream adjacent points~~departure points~~, x_j and x_{j+1}~~x_{dep}~~, is assumed such that

A002

B004

B004

$$u(x) = u(x_j) + (x - x_j)u' \qquad \text{for } x_j \le x \le x_{j+1}, \tag{24}$$

where u' is a constant spatial gradient of the velocity. In order to solve the time evolution of the velocity of a particle at (t_m, x_j), Eq. (24) is differentiated by time t:

$$\frac{\mathrm{d}u}{\mathrm{d}t} = \frac{\mathrm{d}x}{\mathrm{d}t}u' = u'u \,, \tag{25}$$

which is solved as

$$u(t) = u(t_m)\exp\left[u'(t - t_m)\right] \,. \tag{26}$$

Introducing Eq. (26), Eq. (22) is integrated as

$$\langle \xi \rangle = -\int_{t_m}^{t_m+\Delta t} \mathrm{d}t\, u(t) = -u(t_m)\Delta t \left[\frac{\exp(u'\Delta t) - 1}{u'\Delta t}\right] \,, \qquad \text{(when } u' \neq 0\text{)} \tag{27}$$

$$\langle \xi \rangle = -u(t_m)\Delta t \,, \qquad \text{(when } u' = 0\text{).} \tag{28}$$

Based on the above, it can be interpreted that the distance to the departure point is that of constant velocity case (Eq. 23 or 28), multiplied by the bracket term in Eq. (27) as a correction factor. Here, it should be noted that the correction factor reaches 1 toward the limit of $u' \to 0$, which definitely corresponds to the constant velocity case. The velocity gradient u' already appears in the advection equation of the g term (Eq. 4), which is reused in the departure point computation.

2 Model description

2.1 Governing equation

The computation used to determine the age of the ice, i.e., the elapsed time since the ice deposit, is performed with the pure advection equation[1]:

$$\frac{\mathrm{d}\mathcal{A}}{\mathrm{d}t} = 1 \,, \tag{29}$$

where $\mathcal{A}$ is the age and t is time, which is the Lagrangian approach. Eq. (29) is then reformulated into the Eulerian equation for a 1D problem,

$$\frac{\partial \mathcal{A}}{\partial t} + w(z,t)\frac{\partial \mathcal{A}}{\partial z} = 1 \,, \tag{30}$$

where $\mathcal{A} = \mathcal{A}(z,t)$ and $w = w(z,t)$ are the age and vertical velocity fields, respectively, and z is the vertical coordinate. Some models introduce an artificial diffusion term in order to achieve stable integration(e.g., Mügge et al., 1999). However, the pure advection form is kept throughout the present paper. Following most ~~of~~ large-scale numerical ice-sheet models (Greve and Hutter, 1995), the vertical coordinate z is scaled with the local thickness. Introducing the scaled coordinate ζ as

B005

$$\zeta = \frac{z-b}{H} \,, \tag{31}$$

Eq. (30) is reformulated as follows:

$$\frac{\partial \mathcal{A}}{\partial \tau} + \omega\frac{\partial \mathcal{A}}{\partial \zeta} = 1 \,, \tag{32}$$

where $\tau \equiv t$ is the corresponding time coordinate in this system, $b = b(t)$ is the bedrock topography, and $H = H(t)$ is the ice thickness. The new velocity term $\omega = \omega(\zeta,\tau)$ in τ,ζ-system is computed as

$$\omega = w\frac{\partial \zeta}{\partial z} + \frac{\partial \zeta}{\partial t} \,, \tag{33}$$

where derivatives of ζ are computed as:

$$\frac{\partial \zeta}{\partial z} = \frac{1}{H} \,, \tag{34}$$

$$\frac{\partial \zeta}{\partial t} = -\frac{1}{H}\left[\frac{\partial b}{\partial t} + \zeta\frac{\partial H}{\partial t}\right] \,. \tag{35}$$

Since the ice thickness H, which actually reflects the changes in the boundary conditions, may not be constant throughout the time period, $H = H(t)$ is prescribed independently of the boundary conditions in this paper. The surface mass balance term M_s (mass input into the domain), surface evolution, and the vertical velocity at the surface $z = h(t)$ are related as

$$w(z = h(t)) = \frac{\partial h}{\partial t} + M_\mathrm{s}(t) \,, \tag{36}$$

[1]Some models adopt 0 for the right-hand side (e.g., Rybak and Huybrechts, 2003) simply because they use a different age definition. For such cases, redefining $\mathcal{A}$ as $\mathcal{A} - t$ results in an equation that is identical to Eq. (29).

which is derived from the kinematic boundary conditions based on the assumption of a flat surface. The spatial derivative of $\mathcal{A}$ used in the RCIP scheme is derived as follows:

$$\frac{\partial \mathcal{A}'}{\partial \tau} + \omega \frac{\partial \mathcal{A}'}{\partial \zeta} = -\frac{\partial \omega}{\partial \zeta} \mathcal{A}' \,, \tag{37}$$

where $\mathcal{A}' = \frac{\partial \mathcal{A}}{\partial \zeta}$.

In order to solve the time evolution of age and its gradient (Eqs. 32 and 37), the initial and boundary conditions are required. At the free surface $z = h(t)$ (or $\zeta = 1$), a Dirichlet-type boundary condition,

$$\mathcal{A}(\zeta = 1) = 0 \,, \tag{38}$$

holds when the surface mass balance is positive (i.e., $M_\mathrm{s} > 0$). In contrast, when the surface balance is negative, the boundary condition is not necessary, because the departure point of the free surface is inside the ice. A special treatment is required for the zero mass balance at the surface, $M_\mathrm{s} = 0$. In this case, the velocity term in τ, ζ-system, ω becomes 0, so Eq. (3243) is simplified as

B006

$$\frac{\partial \mathcal{A}}{\partial \tau} = 1 \,, \tag{39}$$

which, again, requires no boundary condition for age. The boundary conditions at the bottom $\zeta = 0$ simply mirror those at the surface.

The age derivative, $\mathcal{A}'$, also satisfies the boundary condition at the free surface as

$$\mathcal{A}'(\zeta = 1) = -\frac{1}{M_\mathrm{s}} \,, \tag{40}$$

when $M_\mathrm{s} > 0$. Conditions similar to age hold for the age derivative when $M_\mathrm{s} < 0$ and $M_\mathrm{s} = 0$.

In the present study, equivalent but different coefficient representations~~representation of coefficients~~ (Eqs. 15–19) are adopted for~~on~~ the RCIP method implementation, which is described in Appendix B.

B007

2.2 Discretization

The spatial discretization of Eqs. (32) and (37) can be either uniform or non-uniform. In the present paper, both types of discretization are examined. Since uniform discretization is a special case of non-uniform discretization, the latter can be described effectively without a loss of generality.

One way to introduce a non-uniform discretization is to apply a *non-smooth* grid (Shashkov, 1995), which prescribes irregular discretization of the coordinates:

$$0 \equiv \zeta_0 < \zeta_1 < \cdots < \zeta_{\mathsf{N}_k - 1} \equiv 1 \,, \tag{41}$$

and

$$\Delta\zeta_{k+1/2} = \zeta_{k+1} - \zeta_k \,. \qquad \text{for } k = 0, \cdots, \mathsf{N}_k - 2 \tag{42}$$

Another way to introduce a non-uniform discretization is to apply a *smooth* grid (Shashkov, 1995), which uses a smooth function to transform the coordinate system. One more coordinate transformation is then performed for a non-uniform smooth-grid system as follows:

$$\frac{\partial \mathcal{A}}{\partial \mathsf{T}} + \mathsf{W}\frac{\partial \mathcal{A}}{\partial \mathsf{Z}} = 1\,, \tag{43}$$

$$\frac{\partial \mathcal{A}'}{\partial \mathsf{T}} + \mathsf{W}\frac{\partial \mathcal{A}'}{\partial \mathsf{Z}} = -\frac{\partial \mathsf{W}}{\partial \mathsf{Z}}\mathcal{A}'\,, \tag{44}$$

where T and Z are the time and vertical coordinates in the new system. A smooth transformation of $\mathsf{Z} = \mathsf{Z}(\zeta)$ or its inverse $\zeta = \zeta(\mathsf{Z})$ is prescribed where necessary. Similarly, a new velocity term $\mathsf{W} = \mathsf{W}(\mathsf{Z}, \mathsf{T})$ in T, Z-system is computed as

$$\mathsf{W} = \omega\frac{\partial \mathsf{Z}}{\partial \zeta}\,. \tag{45}$$

Equations (43) and (44), which are the target equations to solve, are simply replacements for Eqs. (32) and (37), respectively. The velocity term $\mathsf{W} = \mathsf{W}(\mathsf{T}, \mathsf{Z})$ is prescribed (as will be explained later). The terms $\mathcal{A}$, W, and 1 on the right-hand side correspond to f, u, and h, respectively, in the RCIP scheme framework (Eq. 1). Although it is possible to introduce further non-uniform discretization on the Z-coordinate, in the present paper, only a uniform discretization is examined on the smooth-grid discretization:

$$\mathsf{Z}_k = \frac{k}{\mathsf{N}_k - 1}\,, \quad \text{for } k = 0, \cdots, \mathsf{N}_k - 1. \tag{46}$$

Actually, the discretization of the ζ-coordinate corresponds to the special case of non-uniform smooth discretization with $\mathsf{Z} \equiv \zeta$. Therefore, for both uniform and non-uniform discretization, the scheme will be described hereafter using the Z-coordinate instead of the ζ-coordinate.

2.3 Comparing other schemes with RCIP schemes

In the present paper, two numerical schemes, the first- and second-order upwind schemes, are examined in comparison with the RCIP schemes. While there are other numerical schemes suitable for such comparisons, including Lagrangian, other semi-Lagrangian, or even higher-order upwind schemes, these have already been reported in past studies (Mügge et al., 1999; Greve et al., 2002; Rybak and Huybrechts, 2003, Clarke and Marshall, 2002,Tarasov and Peltier, 2003; Clarke et al., 2005). Furthermore, since our study focuses on a demonstration of RCIP schemes in relation to the topic of ice dating, a wide range of comparisons is beyond the scope of this paper.

A004

B008

The 'first-order' upwind scheme in the present paper evaluates the advection term using the velocity at staggered grid points as follows:

$$\mathsf{W}\frac{\partial \mathcal{A}}{\partial \mathsf{Z}}\bigg|_{\mathsf{Z}=\mathsf{Z}_k} \simeq \mathsf{W}_{k+1/2}\frac{\mathcal{A}_{k+1} - \mathcal{A}_k}{\Delta \mathsf{Z}_{k+\frac{1}{2}}} = \mathsf{W}_{k+1/2}\mathsf{A}'_{\mathrm{I}}(\mathsf{Z}_{k+\frac{1}{2}})\,, \tag{47}$$

when $\mathsf{W}_{k+1/2} < 0$ and $\mathsf{W}_{k-1/2} < 0$. The velocity at staggered grid points is computed by linear interpolation of the two adjacent velocities at normal grid points. Equation (47) corresponds to numerical integration with the midpoint rule if a Dirichlet-type boundary condition is applied on the upper surface (Eq. 38) and the velocity is kept negative throughout. It is especially

notable that, for ice dating at summits, positive (upward) vertical velocity is rarely considered. Therefore, the mid-point rule formulation mentioned above is sufficient for application. ~~Since, positive vertical velocity is rarely considered for typical ice dating topics, the mid-point rule formulation mentioned above is sufficient for application.~~ On the other hand, a different approach is generally required for a grid point where two velocities at staggered adjacent grid points have opposite signs. In this paper, the velocity term is simply replaced by that at the normal grid point:

B009

$$\mathsf{W}\frac{\partial \mathcal{A}}{\partial \mathsf{Z}}\bigg|_{\mathsf{Z}=\mathsf{Z}_k} \simeq \mathsf{W}_k \mathsf{A'}_{\mathrm{I}}(\mathsf{Z}_{k+\frac{1}{2}}) \,, \tag{48}$$

where $\mathsf{W}_k < 0$, and $\mathsf{W}_{k+1/2}$ and $\mathsf{W}_{k-1/2}$ have opposite signs.

For the 'second-order' upwind scheme, the derivative of the age term is replaced by the second-order upwind difference formulation as

$$\mathsf{W}\frac{\partial \mathcal{A}}{\partial \mathsf{Z}}\bigg|_{\mathsf{Z}=\mathsf{Z}_k} \simeq \mathsf{W}_k \mathsf{A'}_{\mathrm{II}}(\mathsf{Z}_k) \,, \tag{49}$$

where

$$\mathsf{A'}_{\mathrm{II}}(\mathsf{Z}_k) = \frac{(2\Delta\mathsf{Z}_{k+\frac{1}{2}} + \Delta\mathsf{Z}_{k+\frac{3}{2}})\mathsf{A'}_{\mathrm{I}}(\mathsf{Z}_{k+\frac{1}{2}}) - \Delta\mathsf{Z}_{k+\frac{1}{2}}\mathsf{A'}_{\mathrm{I}}(\mathsf{Z}_{k+\frac{3}{2}})}{\Delta\mathsf{Z}_{k+\frac{1}{2}} + \Delta\mathsf{Z}_{k+\frac{3}{2}}} \qquad \text{for } k < \mathsf{N}_k - 2, \tag{50}$$

$$\mathsf{A'}_{\mathrm{II}}(\mathsf{Z}_k) = 2\mathsf{A'}_{\mathrm{I}}(\mathsf{Z}_k) - \mathcal{A'}_{k+1} \,, \qquad \text{for } k = \mathsf{N}_k - 2 \,, \tag{51}$$

for the $\mathsf{W}_k < 0$ case. The age derivative at the surface is required ($\mathcal{A'}_{k+1}$ in Eq. 51), which is provided as a boundary condition (Eq. 40). For higher-order numerical schemes, the introduction of a slope limiter is a standard method for suppressing the development of oscillations near a discontinuity and/or steep gradients (details are described in Greve et al., 2002). Although it is possible to apply such slope limiters in irregular grids (Murman et al., 2005), an easier approach was adopted instead. Specifically, the formulation is switched back to the first-order scheme when $\mathsf{A'}_{\mathrm{I}} > 0 > \mathsf{A'}_{\mathrm{II}}$ or $\mathsf{A'}_{\mathrm{I}} < 0 < \mathsf{A'}_{\mathrm{II}}$. Although this method may be insufficient to stabilize the solution near a strong discontinuity, the implementation of more sophisticated slope limiters is beyond the scope of the present paper.

3 Experiment and Results

3.1 Experimental design

Following some modeling studies on the dating of deep drilling sites that used simplified 1D vertical ice flow models (e.g., Parrenin et al., 2007), the present study adopts an analytical vertical velocity profile under the assumption that there are no horizontal variations in the bedrock elevation, surface, and basal mass balances:

$$w(\zeta) = -\left[\left(M_{\mathrm{s}} + M_{\mathrm{b}} - \frac{\partial H}{\partial t}\right)\tilde{w}(\zeta) - M_{\mathrm{b}}\right] \,, \tag{52}$$

where M_{s} and M_{b} are the surface and basal mass balance (positive is input), respectively, H is the ice thickness, and $\tilde{w}(\zeta)$ is the normalized velocity profile. Assuming no basal sliding, $\tilde{w}(\zeta)$ can be approximated by

$$\tilde{w}(\zeta) = 1 - \frac{p+2}{p+1}(1-\zeta) + \frac{1}{p+1}(1-\zeta)^{p+2} \,, \tag{53}$$

where p is a parameter for the profile (Parrenin et al., 2007). Under the Glen's flow law with a steady-state isotropic ice condition, p is equal to the flow law exponent n (typically $n = 3$). In addition, the RCIP scheme requires the derivative of the velocity, which is computed using the derivative of $\tilde{w}$, as

$$\frac{\partial \tilde{w}}{\partial \zeta} = \frac{p+2}{p+1}\left[1-(1-\zeta)^{p+1}\right] . \tag{54}$$

In addition to the vertical velocity, the time evolutionsevolution of the surface and basal mass balances and the ice thickness are required for the age computations. These will be presented in each of the following sections.

The initial conditions forof the $\mathcal{A}$ and $\mathcal{A}'$ fields are set to 0 for all our experiments. In these cases, the age derivative $\mathcal{A}'$ is kept 0 under the level at which the age reaches the integration time. Starting from the 0 field, time integration is computed for 2000 kyr for most of our experiments.

It is worth mentioning that formulations like Eq. (52), which is a function of normalized depth, make it possible to interpret example results for different configurations when appropriate spatial/temporal dimension scaling is used. In this case, the spatial and temporal characteristic scales can be defined, for example, by the ice thickness and the surface mass balance. This means that the age solution under the configuration of 3 and $0\,\mathrm{cm\,yr^{-1}}$ for the surface and basal mass-balance, respectively, has the same normalized shape as that under 30 and $0\,\mathrm{cm\,yr^{-1}}$, by scaling all the time-related terms as $1/10$. B4,B017

All the computationscomputation in our present study were performed on a personal computer (PC) equipped with an Intel Xeon E5-2609 central processing unit (CPU) and compiled with GNU Fortran. Each surface/basal mass balance, ice thickness, and vertical resolution configuration is repeated using four numerical schemes: the RCIP with departure correction (RCIP+corr), the RCIP without correction (RCIP), the second-order upwind scheme (UP-2), and the first-order upwind scheme with mid-point rule (UP-1). Additionally, athe first-order scheme without a mid-point rule (UP-1n) is sometimes used. Multiple 1D-column experiments with different boundary configurations using one numerical scheme are examined simultaneously in one run. For example, the mean computational costs for one run (with 28 different configurations) in the case of 129 levels over 200 kyr are 30, 28, 32, and 34 seconds, using UP-1, UP-2, RCIP, and RCIP+corr, respectively. Those in the case of 513 levels are 338, 296, 364, and 392 seconds, respectively. Details differ among the configurations, and it takes 30 to 40% more time to perform a RCIP+corr run than to perform a UP-2 or UP-1 run. B010 A2

3.2 A verification experiment using uniform velocity

Before performing an experiment under a typical ice sheet configuration, verification of the numerical model used in the present study is presented under further simplified conditions, namely, the constant velocity case. This is easily performed using Eq. (52), in which the parenthesis term equals 0, in other words, by keeping H constant and arbitrarily setting $M_\mathrm{s} \equiv -M_\mathrm{b}$ for arbitrarily p. B011

Figure 2 shows the computed age profile under the uniform velocity of $-15\,\mathrm{cm\,yr^{-1}}$ and $H = 3000\,\mathrm{m}$. Uniform grid spacing of 129 levels is adopted, which corresponds to $\mathsf{Z} \equiv \zeta$ and $\Delta\mathsf{Z} = \Delta\zeta = 1/2^7$ (i.e., $\Delta z = 23.4375\,\mathrm{m}$) using the smooth grid. The time step is set as 100 yr, which corresponds to the Courant–Friedrichs–Lewy (CFL) condition ~ 0.64. The vertical age profile 1

is formulated as

$$\mathcal{A}(z,t) = \min\left[t, \int_h^z \mathrm{d}z' \frac{1}{w}\right] , \tag{55}$$

thus the exact solution for an uniform velocity is

$$\mathcal{A}(z,t) = \min(t, -z/w_c) , \tag{56}$$

where $w_c = -15\,\mathrm{cm\,yr^{-1}}$. For completion purposes, the results of the RCIP scheme are plotted in the figure, which is (by definition) identical to those of RCIP+corr scheme. For the steady state, a linear age profile from $0\,\mathrm{yr}$ at the surface and $20\,\mathrm{kyr}$ at the bottom is expected (corresponding to the thick gray line in Fig. 2), which is obtained by all the methods after integration of around $27\,\mathrm{kyr}$ (not shown). In contrast, the transient states are different among the results of the four schemes examined. Figure 3 shows the computed age profile relative to the exact solution, with three different time steps, 100, 50, and $25\,\mathrm{yr}$, for each scheme. The results of RCIP+corr (and thus RCIP) are shown to be less sensitive to the time step than the upwind schemes, which reflects the fact that both the interpolation and the departure point calculation are successful. At $20\,\mathrm{kyr}$, a linear age profile should be obtained, but all four results show ages that are younger than the exact solution, due to numerical diffusion. Additionally, while all of the schemes show relatively good performance for the upper part, the result obtained by the UP-1 scheme deviates the most from the solution. Specifically, it deviates $1\,\mathrm{yr}$ from around $2/3$ of the total depth and reaches almost $1\,\mathrm{kyr}$ at the bottom, which is already visible in Fig. 2. In contrast, the other results deviate from the solution only near the bottom ~~$\sim 9/10$ around 9/10~~ of the total depth, and reach ~~$\sim 100\,\mathrm{yr}$ around 100 yr~~, or even less, at the bottom. The error at the bottom of UP-1 is 759 to $902\,\mathrm{yr}$ (3.8 to 4.5%), while that of RCIP is 76 to $98\,\mathrm{yr}$ (0.38 to 0.49%), and the best of UP-2 is even better at 7.5 to $154\,\mathrm{yr}$ (0.04 to 0.77%).

1 2 1 B012

3.3 Experiment with steady non-uniform vertical velocity

Hereafter, non-uniform velocity experiments are performed using $p = n = 3$ in Eq. (53). First, simple cases with constant surface/basal mass balances, as well as thicknesses that correspond to steady vertical velocity profiles, are shown. Since Eq. (55) cannot be solved using (52), profiles created by numerical integration (the Runge–Kutta scheme) are used as 'benchmark' solutions in this and the following section.

The ice thickness and the accumulation rate chosen in this and the following sections are $\sim 3000\,\mathrm{m}$ and $\sim 3\,\mathrm{cm\,yr^{-1}}$, respectively, which correspond to typical quantities for the East Antarctic Plateau during the glacial period (e.g., Parrenin et al., 2007; Fischer et al., 2013). On the other hand, there are other cases with similar thicknesses and ten-times higher accumulation ($\sim 30\,\mathrm{cm\,yr^{-1}}$), typically in Greenland or West Antarctica (e.g, Clarke and Marshall, 2002). As mentioned in Sect. 3.1, with proper scaling, the results in these sections can be interpreted as results with such higher accumulation rates. This will be examined in the Discussion (Sect. 4).

B4,B017

Two sets of basal melting are presented: no basal melting and $3\,\mathrm{mm\,yr^{-1}}$. The other two parameters are fixed. Surface mass balance is set as $3\,\mathrm{cm\,yr^{-1}}$ and thickness is set as $H = 3000\,\mathrm{m}$. We use a uniform ~~Uniform~~ grid spacing of 129 levels ($\Delta z = 23.4375\,\mathrm{m}$), and the time step is set as $100\,\mathrm{yr}$, which is the same configuration used in the previous section.

B013

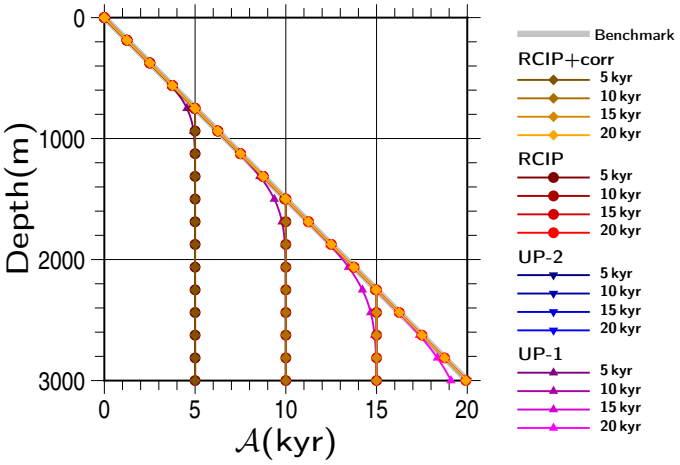

Figure 2~~1~~. Experimental results obtained using a uniform velocity of $w = 15\,\mathrm{cm\,yr^{-1}}$. Snapshots of the computed vertical age profiles obtained by RCIP with correction, RCIP, second-, and first-order upwind schemes at $t = 5, 10, 15, 20\,\mathrm{kyr}$ are shown. Since the 'correction factor' of the departure points is 1 (Eq. 28), the results of RCIP with correction are identical to those of RCIP. The results of the second-order upwind scheme are close to those of the RCIP, which are barely visible in this scale. The solution is also shown as a benchmark (thick gray line). Symbols are plotted for every eight vertical levels.

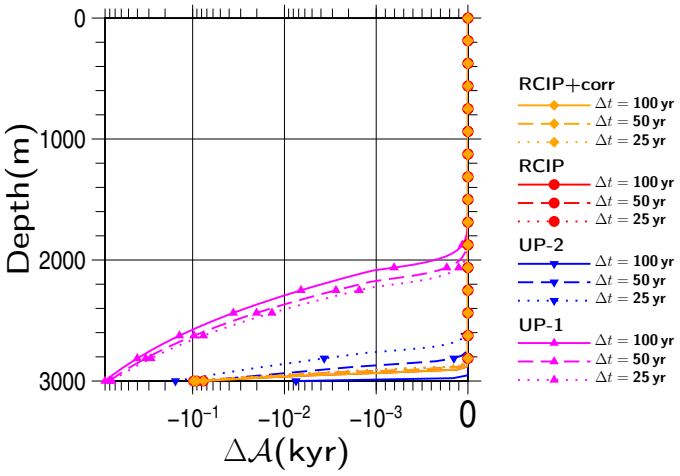

Figure 3~~2~~. Experimental results obtained using a uniform velocity of $w = 15\,\mathrm{cm\,yr^{-1}}$. Snapshots of computed vertical age profiles obtained by RCIP with correction, RCIP, ~~and~~ second-, and first-order upwind schemes at $t = 20\,\mathrm{kyr}$ relative to the exact solution are shown. The results of different time steps of 100, 50, and 25, yr are shown for each scheme. The results of RCIP with correction are identical to those of RCIP. Age differences are shown on a logarithmic scale, except for those near 0, which are shown on a linear scale. Symbols are plotted for every eight vertical levels.

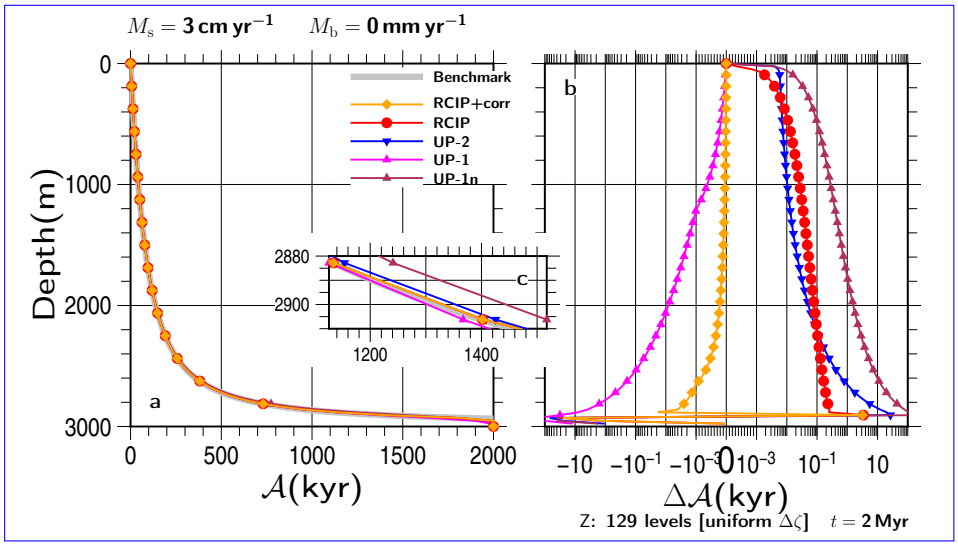

Figure 4~~3~~. Experimental results obtained under steady vertical velocity profiles with $H = 3000\,\mathrm{m}$, $M_s = 3\,\mathrm{cm\,yr^{-1}}$ and $M_b = 0\,\mathrm{mm\,yr^{-1}}$. (a) Computed vertical age profiles by RCIP with departure point correction (RCIP+corr), the RCIP scheme, the second-order upwind scheme (UP-2), the first-order upwind scheme (UP-1), and the first-order upwind scheme without the mid-point rule (UP-1n) at $t = 2000\,\mathrm{kyr}$, (b) those relative to the *benchmark* profile obtained by numerical integration, and (c) a zoomed-in portion of the bottom part of (a) showing that the differences among the experiments is on the order of 10 kyr. Age differences are shown on a logarithmic scale, except for those near 0, which are shown on a linear scale. Uniform grid spacing of 129 levels is adopted in this simulation. B014

Figures 4a and 5a show computed age profiles at $t = 2000\,\mathrm{kyr}$ for all the schemes along with the *benchmark* age profiles. 4
Very few differences can be seen among the profiles over most parts of the figures under this scale. Deviations from the benchmark are shown in Figs. 4b and 5b. The results of each scheme show larger errors near the bottom than near the upper 4
315 part. Some results show sudden increases in the error at certain depths, which correspond to the depths around where the age should reach the time of integration.

The RCIP+corr scheme shows the best result for all depths. The UP-1 scheme shows the second-best result, which is even better than the RCIP scheme around the depth of 2600 m. However, it also shows the largest errors among all the schemes examined at deeper depths. The good performance of UP-1, in spite of its smallest spatial accuracy, which is attributed to the
320 cancellation of errors due to discretization and numerical diffusion, has already been presented in Greve et al. (2002). The mid-point rule formulation (Eq. 47) also plays a role in the increased accuracy. Due to simple situations, such as the one-direction advection and the constant upper boundary conditions, the age profile computation can be formulated as a vertical integration B015 from top to bottom. This means that the mid-point rule integration actually has second-order accuracy. A *true* first-order upwind scheme can be applied by using Eq. (48) over the whole domain. In this case, vertical integration from top to bottom
325 corresponds to an Euler integration, which has first-order accuracy. Figures 4b and 5b also contain results obtained using such 4
a scheme, marked as UP-1n. However, as expected, when such a normal-grid velocity is introduced for the advection equation,

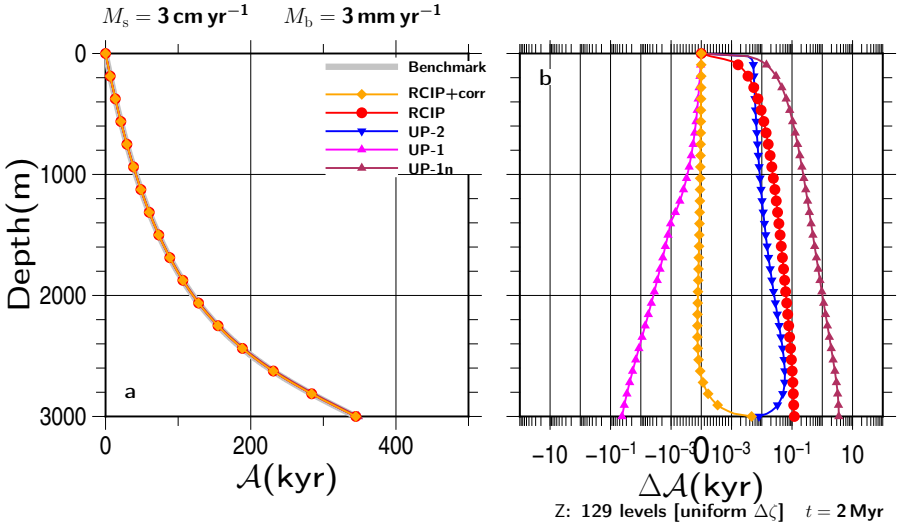

Figure 5 ~~4~~**.** Same as Fig. 4a, b, except for the experiment with $M_\mathrm{b} = 3\,\mathrm{mm\,yr^{-1}}$. B014

the results have less accuracy than those of the second-order upwind (UP-2). Furthermore, as shown in Greve et al. (2002), the improved performance of the UP-1 scheme is limited to the upper part, and the errors become larger as the depth increases. The results of the RCIP scheme show relatively larger errors than the other methods, except for the top and the bottom part, which highlights the importance of accurate departure point calculations. The result of the UP-2 scheme shows intermediate errors between RCIP and UP-1 at the bottom.

3.4 Non-steady surface mass balance experiments

This section presents the results of experiments conducted with non-steady velocity profiles, which were performed with the prescribed surface mass balance time series. First, a very simple square-wave formulation is adopted for the time evolution of B016 the surface mass balance.

$$\begin{cases} M_\mathrm{s}(t) = a_\mathsf{H}\,, & (0 \le \mod(t, P_\mathsf{T}) < P_\mathsf{H}) \\ M_\mathrm{s}(t) = a_\mathsf{L}\,, & (P_\mathsf{H} \le \mod(t, P_\mathsf{T}) < P_\mathsf{T} = P_\mathsf{H} + P_\mathsf{L}) \end{cases} \tag{57}$$

where a_H and a_L are the prescribed high and low surface mass balance terms, P_H and P_L are the durations with high- and low-value phases, and P_T is the duration of one cycle. Figure 6 shows the time evolution of a normalized surface mass balance 5 with $P_\mathsf{T} = 100\,\mathrm{kyr}$ cycles and a phase pattern of $P_\mathsf{H}, P_\mathsf{L}$=1 : 1 as an example. Several experimental configuration combinations are examined, including $P_\mathsf{H}, P_\mathsf{L}$=1 : 1, 7 : 1, or 1 : 7; and $M_\mathrm{b} = 0, 0.3$, or $3\,\mathrm{mm\,yr^{-1}}$. The other patterns examined in this paper are provided as a supplement~~Supplement~~ to this paper.

Figures 7 and 8 show computed age profiles at $t = 1000\,\mathrm{kyr}$ under the square-wave surface mass balance, where the lower 7 surface mass balances are set as $a_\mathsf{L} = 1.5\,\mathrm{cm\,yr^{-1}}$ and $0.75\,\mathrm{cm\,yr^{-1}}$. The higher surface mass balances and the basal are set as $a_\mathsf{H} = 3\,\mathrm{cm\,yr^{-1}}$ and $M_\mathrm{b} = 0$, respectively. For reference purposes, the benchmark solutions with constant surface mass

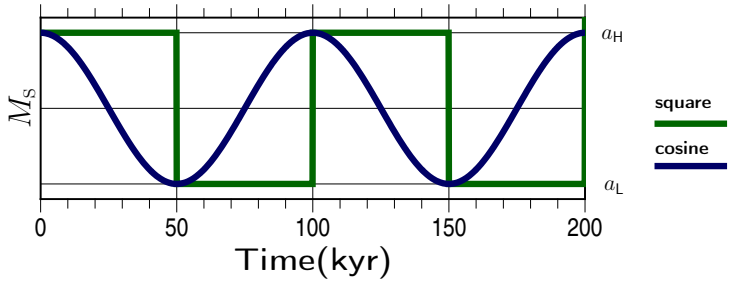

Figure 6 5. Schematic figure showing the time evolution of the surface mass balance adopted in these experiments. Only the first two cycles are plotted.

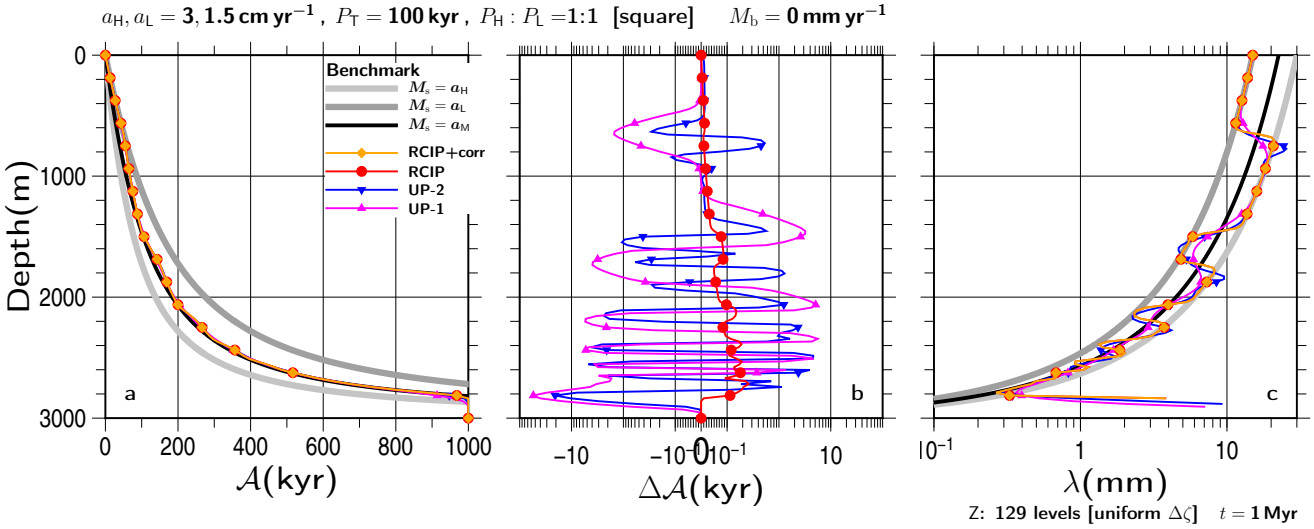

Figure 7 6. Results of transient experiments with square-wave surface mass balances of $a_H, a_L = 3, 1.5\,\mathrm{cm\,yr^{-1}}$, $P_T = 100\,\mathrm{kyr}$, $P_H : P_L = 1:1 = 50:50\,\mathrm{kyr}$, square-wave, $M_b = 0$, and constant $H = 3000\,\mathrm{m}$. (a) Vertical profiles of the computed age and (c) annual layer thickness at $1000\,\mathrm{kyr}$ using RCIP+corr, RCIP (overlapped on RCIP+corr), UP-2, and UP-1 are shown. The last $500\,\mathrm{yr}$ is clipped from (c), where the age gradient (inverse of λ) is close to 0 reflecting the initial condition. (b) The computed age differences at the same depth relative to the result of the RCIP+corr case are shown on a logarithmic scale, except for those near 0, which are shown on a linear scale. For reference purposes, the gray lines indicate benchmark solutions for the constant surface mass balance cases of a_H, a_L, and a_M. Uniform grid spacing of 129 levels is adopted in this simulation.

balances of a_H and a_L are shown with gray lines. The black line is the benchmark solution with the constant surface mass balances of the mean, $a_M = (a_H + a_L)/2$. As shown in these figures, the computed age profiles are close to the benchmark solution with a_M, particularly at the bottom. For the upper part, the computed age profiles are along the benchmark solutions for the constant surface mass balance cases of a_L.

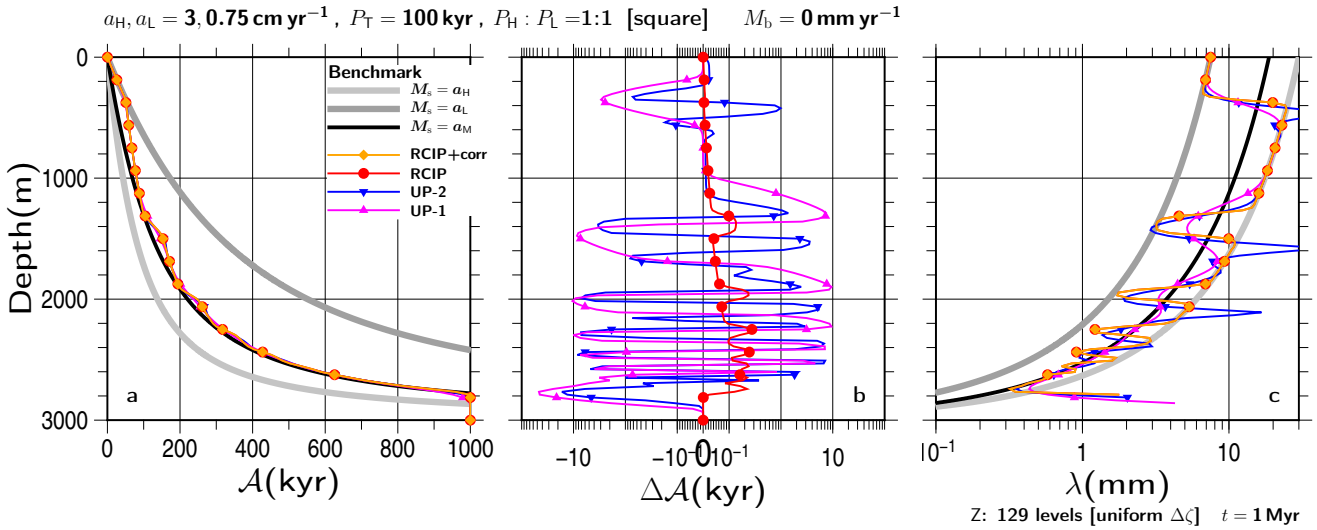

Figure 8 ~~7~~. Same as Fig. 7, but for the results of transient experiments using a square-wave surface mass balance of $a_L = 3, 0.75\,\mathrm{cm\,yr^{-1}}$. 6

Since there are few visible differences among the computed ages, the computed age profiles relative to the one produced by the RCIP+corr scheme (Fig. 7b) are shown. The figures show comparable relative performance levels in spite of the different 6
input surface mass balance histories. The age profiles produced by the RCIP scheme deviate systematically from RCIP+corr by less than $1\,\mathrm{kyr}$ throughout the depth range, which reflects the differences in computing the departure points. The other two schemes deviate around $10\,\mathrm{kyr}$ at most. The age difference oscillations seen in the UP-2 and UP-1 schemes are visible near the age corresponding to the time when switching was conducted between the high and low surface mass balances. ($\Delta\mathcal{A}$ vs. $\mathcal{A}$ plots are presented in the Supplement). These oscillations reflect the characteristics of the UP-2 and UP-1 schemes at the discontinuities.

Figures 7c and 8c show the computed annual layer thickness, λ, against the depth. In the present paper, the annual layer 7
thickness is defined as the inverse of the age gradient. For the RCIP+corr and RCIP methods, the computed field of the age derivative itself ($\mathcal{A}'$ in Eq. 44) is used with the coordinate transformation. On the other hand, for the UP-2 and UP-1 methods, the diagnosed field is used (A'_{I} or $\mathrm{A}'_{\mathrm{II}}$ in Eqs. 47,50,51, respectively). An infinite or a very large annual layer thickness may be present near the bottom, due to the zero gradient of age as a consequence of the initial experiment conditions. In this study, the last $500\,\mathrm{yr}$ is clipped from the figures.

The annual layer thickness has the following relationship in terms of the thinning rate:

$$\frac{\partial \lambda}{\partial t} = \frac{\partial w}{\partial z}\lambda \tag{58}$$

while assuming that layers remain horizontal (Cuffey and Paterson, 2010). When the basal mass balance is 0 and the thickness is constant, the vertical velocity gradient can be formulated from Eq. (52) as

$$\frac{\partial w}{\partial z} = -M_s \frac{\partial \tilde{w}}{\partial \zeta}\,. \tag{59}$$

Finally after some derivation, the vertical gradient of annual layer thickness can be formulated as

$$\frac{\partial \lambda}{\partial z} = \frac{\lambda}{\tilde{w}} \frac{\partial \tilde{w}}{\partial \zeta} , \tag{60}$$

which is a function of λ and the normalized vertical velocity shape. This experiment was conducted with zero basal mass balance, constant thickness, and the same normalized velocity. Therefore, the vertical profile of the annual layer thickness should go back and forth on the two lines produced by those computed using the constant surface mass balances.

In terms of computed annual layer thickness profiles, the RCIP+corr and RCIP (which overlap with RCIP+corr in the figure) methods show particularly good performance over the upper part, as shown in Figs. 7c and 8c. Dissipation at the discontinuity becomes larger towards the bottom, but the solution of RCIP+corr (RCIP) is somewhat more stable on the two benchmark lines than the other schemes. Overshooting at the discontinuity is shown for the solution by the UP-2 scheme, which becomes larger as the difference between the high and low surface mass balances increases. In the present study, this is considered to be a consequence of an inadequate slope filter. In addition, the annual layer thickness is diagnosed with Eq. (50) for the UP-2 scheme, which may exaggerate the oscillation of age gradients more than the simple first-order Taylor expansion. For the UP-1 scheme results, the annual layer thickness diffuses with the depth level and approaches the constant accumulation case of its mean. In deeper areas, the annual layer thickness is found in the vicinity (above or below) of the mean a_{M} benchmark profile in all of the numerical schemes.

The same exercises were performed using a different shape for the time evolution of the surface mass balance. Figure 9 shows the results for ~~Figures 8 and 9 are the results of~~ an experiment conducted using the cosine-wave formulation of the surface mass balance (Fig. 6), which is relatively more continuous than the square-wave version. Similar performance levels were obtained by the UP-2 and RCIP+corr (RCIP) methods for the small amplitude case (Fig. 9c). Instability also arises at low-to-high transitions when the ratio of high/low accumulation is larger (archived in the Supplement) ~~(Fig. 9c)~~.

Figure 10 shows the results obtained by square-wave forcing in terms of computed annual layer thickness, λ, against the computed age for all the schemes, obtained by the relative duration of the $P_{\mathrm{H}} : P_{\mathrm{L}} = 1 : 1$ case (similar figures obtained by other experimental configurations are archived in the Supplement). Since the periodicity of the input cycle is $100\,\mathrm{kyr}$ in this experiment, the annual layer thickness profiles should show the same periodicity. The obtained results show relatively good performance for the RCIP+corr(RCIP) scheme in terms of the phases when compared with the UP-2 and UP-1 schemes. Dissipation at the discontinuity blur the square-wave shapes, particularly at the deeper part, but the phases are still maintained better by the RCIP+corr (RCIP) scheme than by the UP-2 scheme.

3.5 Non-steady thickness experiments

The time evolution of the surface mass balance often involves the evolution of ice thickness as a response. In this section, age computation performance levels under non-steady mass balance and ice thickness conditions are presented. In the present paper, the time evolution of thickness is computed as follows:

$$\frac{\partial H}{\partial t} = -\frac{1}{\tau_H} \{ H - \mathrm{H}_{\mathrm{ref}}(M_{\mathrm{s}}) \} , \tag{61}$$

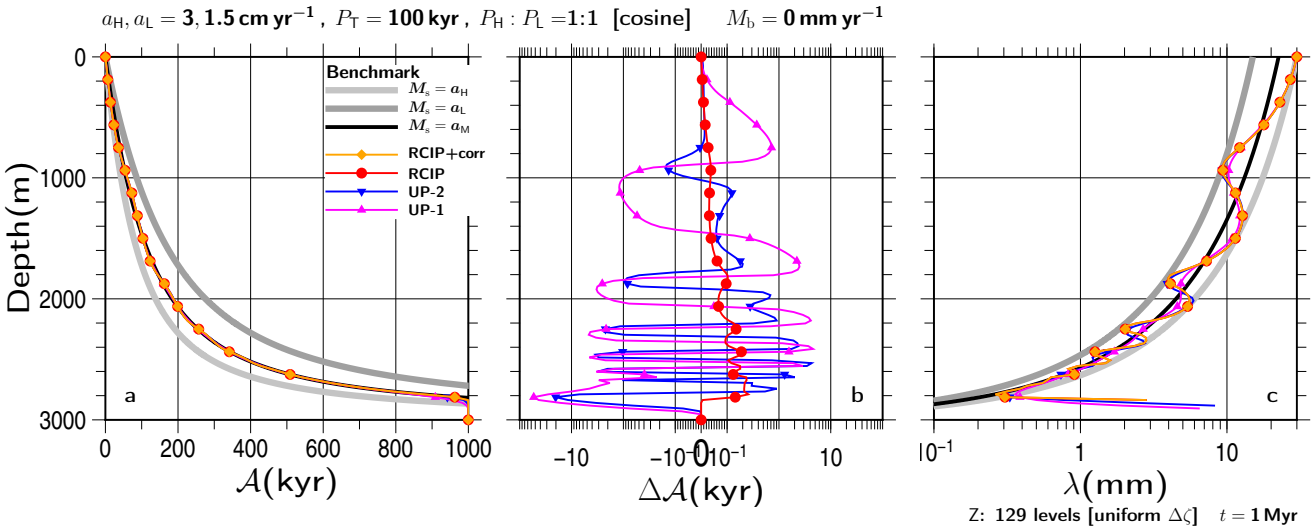

Figure 9 ~~8~~. Same as Fig. 7, but for the results of transient experiments conducted with a cosine-wave surface mass balance of $a_H, a_L = 3, 1.5\,\mathrm{cm\,yr^{-1}}$.

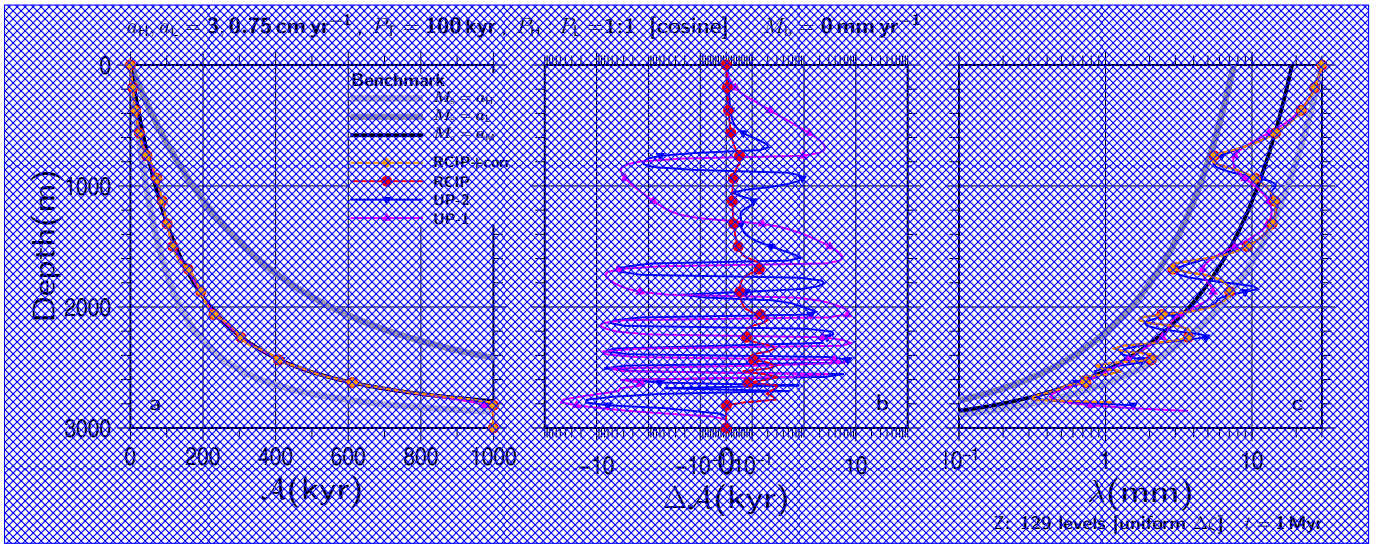

Figure ~~9~~. ~~Same as Fig. 6, but for the results of transient experiments conducted with a cosine-wave surface mass balance of $a_H, a_L = 3, 0.75\,\mathrm{cm\,yr^{-1}}$.~~

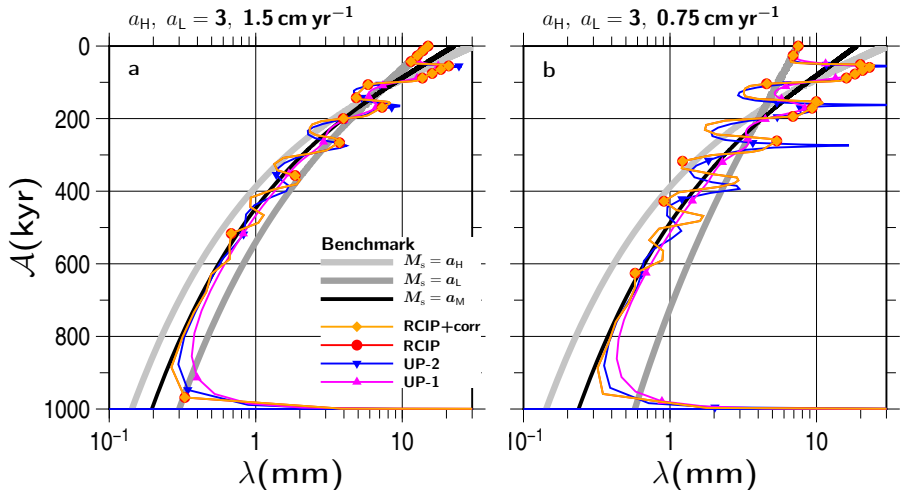

Figure 10. Results of transient experiments with square-wave surface mass balances of (a) $a_H, a_L = 3, 1.5\,\mathrm{cm\,yr^{-1}}$ and (b) $3, 0.75\,\mathrm{cm\,yr^{-1}}$ with high- and low-value phase durations (Eq. 57) set as $P_H : P_L = 1 : 1 = 50 : 50\,\mathrm{kyr}$. The basal mass balances are set as 0. The computed annual layer thickness of λ against the computing age is shown (RCIP overlaps with RCIP+corr). The gray lines indicate benchmark solutions of the constant surface mass balance cases of a_H and a_L, while the black lines $a_M = (a_H + a_L)/2$ are provided as references. Uniform grid spacing of 129 levels is adopted in this simulation.

where $\mathsf{H}_{\mathrm{ref}}(M_s)$ is the reference thickness as a function that depends solely on the surface mass balance and τ_H is the response thickness timescale. Under ideal conditions~~an idealized condition~~, the steady-state ice thickness at the summit is proportional to the $1/(2n+2)$ power of the surface mass balance, where n is the Glen's flow low exponent (Cuffey and Paterson, 2010). Following this relationship, the reference thickness is formulated as

$$\mathsf{H}_{\mathrm{ref}}(M_s) = H(t=0)\left[\frac{M_s(t)}{M_s(t=0)}\right]^{1/(2n+2)} . \tag{62}$$

For cases where $H(t=0) = 3000\,\mathrm{m}$, $a_H, a_L = 3, 1.5\,\mathrm{cm\,yr^{-1}}$ and $P_T = 100\,\mathrm{kyr}$, the evolution of H over the first two cycles can be computed as shown in Fig. 11 using Eqs. (61) and 62. The lower thickness limit in this case is $3000 \times (1.5/3.0)^{1/8} \sim 2751.01\,\mathrm{m}$.

Several experimental configuration combinations are examined. These include square-wave or cosine-wave forcing; $a_H, a_L = 3, 1.5\,\mathrm{cm\,yr^{-1}}$ or $3, 0.75\,\mathrm{cm\,yr^{-1}}$; $\tau_H = 3\,\mathrm{kyr}$ or $10\,\mathrm{kyr}$; P_H, P_L=1 : 1, 7 : 1, or 1 : 7; $M_b = 0$, 0.3, or $3\,\mathrm{mm\,yr^{-1}}$. Figure 12 shows the result~~Figures 12 and 13 are the results~~ of experiments conducted with response time scales of $10\,\mathrm{kyr}$ for the~~under~~ $100\,\mathrm{kyr}$ cycle square-wave case provided as an example~~and with cosine-wave forcing cases provided as examples~~. The gray lines in the figures are the benchmark solution with constant surface mass balances of a_H and a_L and their corresponding reference thickness of $\mathsf{H}_{\mathrm{ref}}$. The black line is computed using the mean surface mass balance $a_M = (a_H + a_L)/2$, and the mean thickness over the last cycle of its evolution.

B3

B3

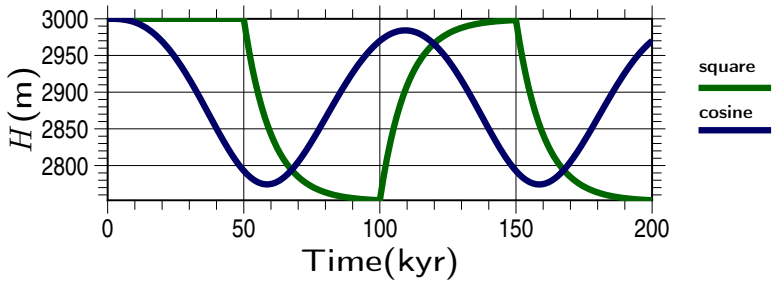

Figure 11. Prescribed time evolution patterns of ice thickness adopted in the non-steady thickness experiment. The thickness evolution ~~evolution of thickness~~ is computed using ~~anthe~~ e-folding time of $10\,\mathrm{kyr}$ against square-wave and cosine-wave formulation of the surface mass balance with $a_\mathrm{H}, a_\mathrm{L} = 3, 1.5\,\mathrm{cm\,yr^{-1}}$ (Fig. 6) provided as an example.

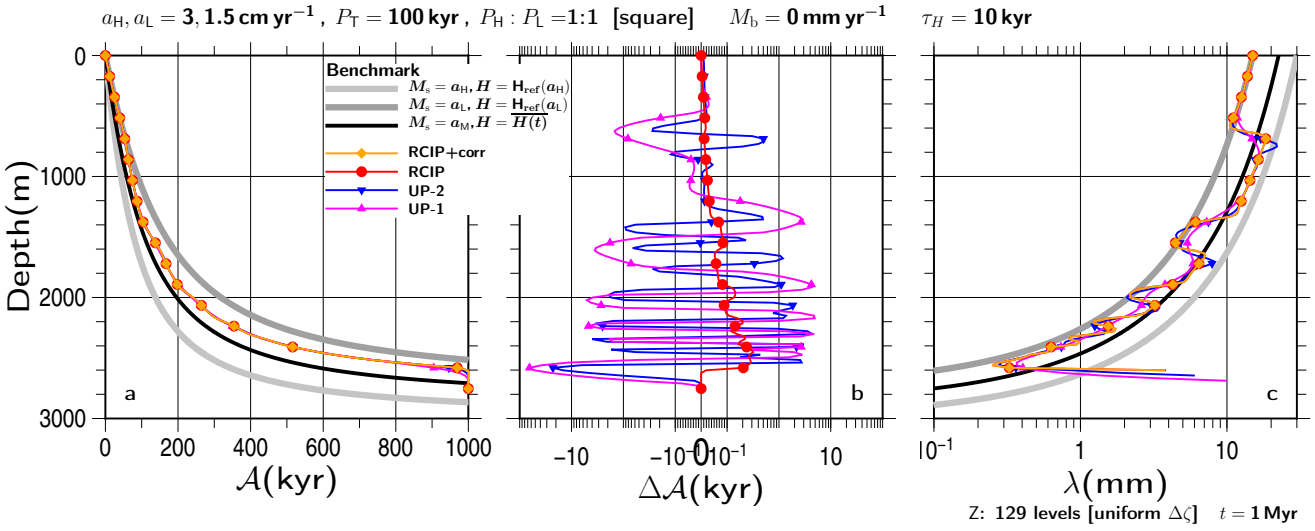

Figure 12. Same as Fig. 7, but for the results of non-steady thickness experiments conducted with the response timescale set as $\tau_H = 10\,\mathrm{kyr}$. The reference thickness values H for the benchmark profiles are explained in the text.

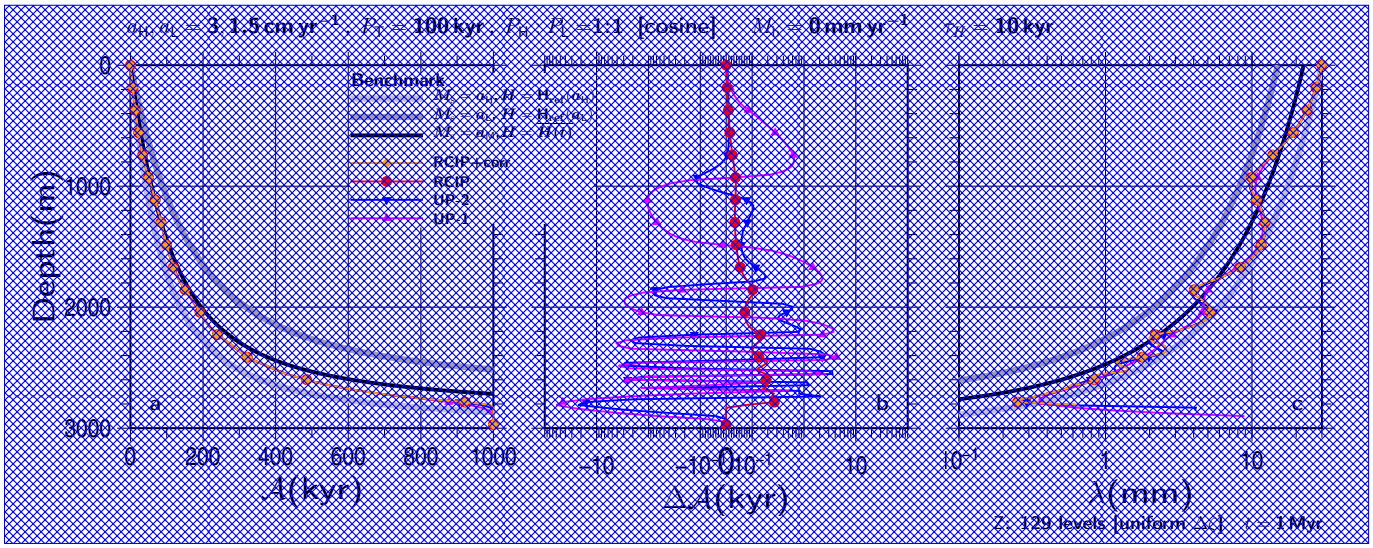

Figure ~~13. Same as Fig. 8, but for the results of non-steady thickness experiments conducted with the response timescale set as $\tau_H = 10$ kyr. The reference thickness values H for the benchmark profiles are explained in the text.~~ B3

A comparison with the fixed thickness experiments (Fig. 7 vs Fig. 12, or other combinations archived in the Supplement) 6 (~~Figs. 6 and 8 vs Figs. 12 and 13~~) shows~~show~~ no significant differences. The preservation of discontinuity in the annual layer B3 thickness is similar to that seen in the non-steady thickness case. The differences in computed age, as well as the performance levels of the phases in the annual layer thickness, are qualitatively the same. In addition, all of the combinations examined in this paper show corresponding results that are qualitatively similar to those obtained in the fixed thickness experiments.

3.6 Occasional non-positive surface mass balance experiments

So far, the surface mass balance values adopted in our experiments have been positive (corresponding to the accumulation zone). This limitation is sufficient for the usual topics relating to deep ice-core experiments, where the interpretation of ice-core data may become too complex. However, in order to provide a complete demonstration of the performance levels of numerical age computations for more general cases, it is worthwhile to examine other cases. Although it may be considered pointless to examine steady negative mass balance cases because they simply mirror the steady positive cases presented above, the surface mass balance level adopted in this section is examined with zero or negative a_L in Eq. (57) and Fig. 6. One 5 encountered difficulty is computing vertical velocity when the surface mass balance is negative. Strictly speaking, it is possible to apply negative M_s to Eqs. (52) and (53), but the validity of such a formulation may be questionable because it is based on an idealized steady-state ice-sheet solution under positive surface mass balance conditions (e.g., Rybak and Huybrechts, 2003). However, for the sake of simplicity, the vertical velocity profiles in the current study are prescribed using the same set of

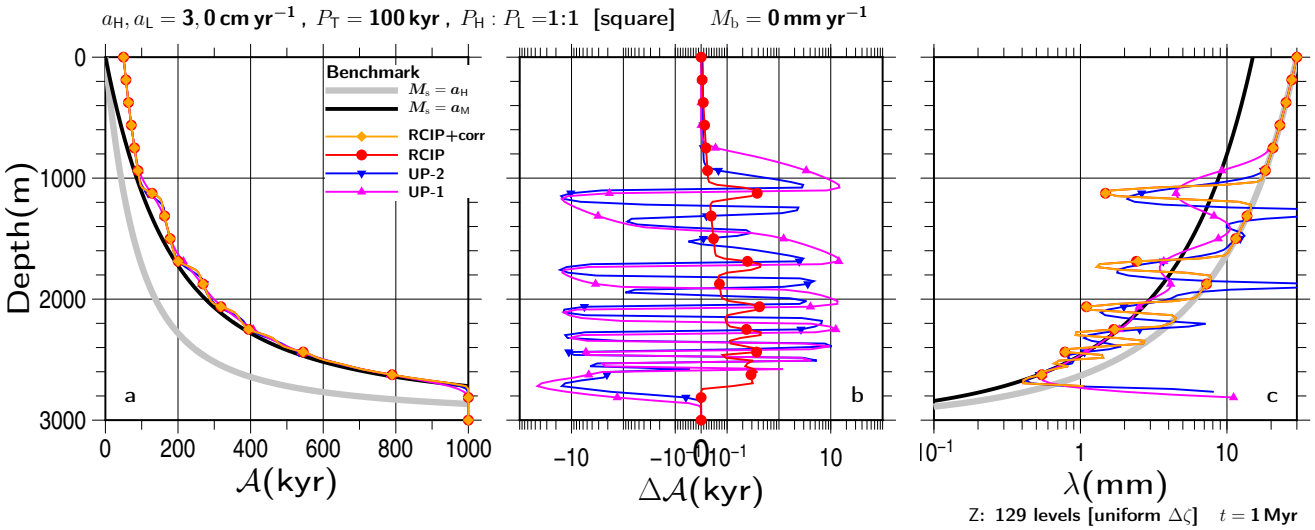

Figure 13 ~~14~~**.** Same as Fig. 7, but for the results of transient experiments conducted using a square-wave surface mass balance with $a_L = 0\,\mathrm{cm\,yr^{-1}}$. 6

equations for both positive and negative surface mass balances. This is considered to be sufficient, particularly for evaluations of the numerical performance levels of different schemes~~scheme numerical performance levels~~. B019

The results of the transient experiments that were conducted under a square-wave surface mass balance of $a_L = 0\,\mathrm{cm\,yr^{-1}}$ are presented in Fig. 13, while the other configuration is the same as in Figs. 7 and 8.~~Figure 14 is the result of transient~~ 7

435 ~~experiments conducted under the square-wave surface mass balance of $a_L = 0\,\mathrm{cm\,yr^{-1}}$, while the other configuration is the same as Fig. 6 or 7.~~ The results obtained under a configuration with $a_L = -1.5\,\mathrm{cm\,yr^{-1}}$ are archived in the Supplement. A005

~~Figure 15 is a configuration with $a_L = -1.5\,\mathrm{cm\,yr^{-1}}$.~~ For both experiments, the~~The~~ thickness is fixed as 3000 m, the mass A005

balances are $a_H = 3.0\,\mathrm{cm\,yr^{-1}}$, $M_b = 0$, and the phases are $P_H, P_L = 50, 50\,\mathrm{kyr}$.

Several experimental configuration combinations are examined. In a comparison involving~~with~~ the experimental results of

440 the positive mass balance cases examined in this paper, qualitatively similar results are presented. As the prescribed surface mass balance at the lower a_L becomes smaller, errors in the annual layer thickness become clearer around the middle depth. The λ for~~by~~ the RCIP+corr(RCIP) scheme at the 1600 m depth and below does not extend to the reference gray line (Fig. 13c) 14

~~(Figs. 14c and 15c)~~. This is due to the lack of sufficient vertical resolution when capturing the variation. However, the results B3

are still better than those obtained from the other schemes.

445 **3.7 Resolution**

Annual layer thickness becomes smaller with depth, which reflects the vertical velocity profile. Therefore, differences in age between two neighboring levels become larger with increasing depth. At a certain depth, the grid spacing becomes insufficient to hold the variation of the input age cycles, which means that the preservation of the input variation is lost below that depth.

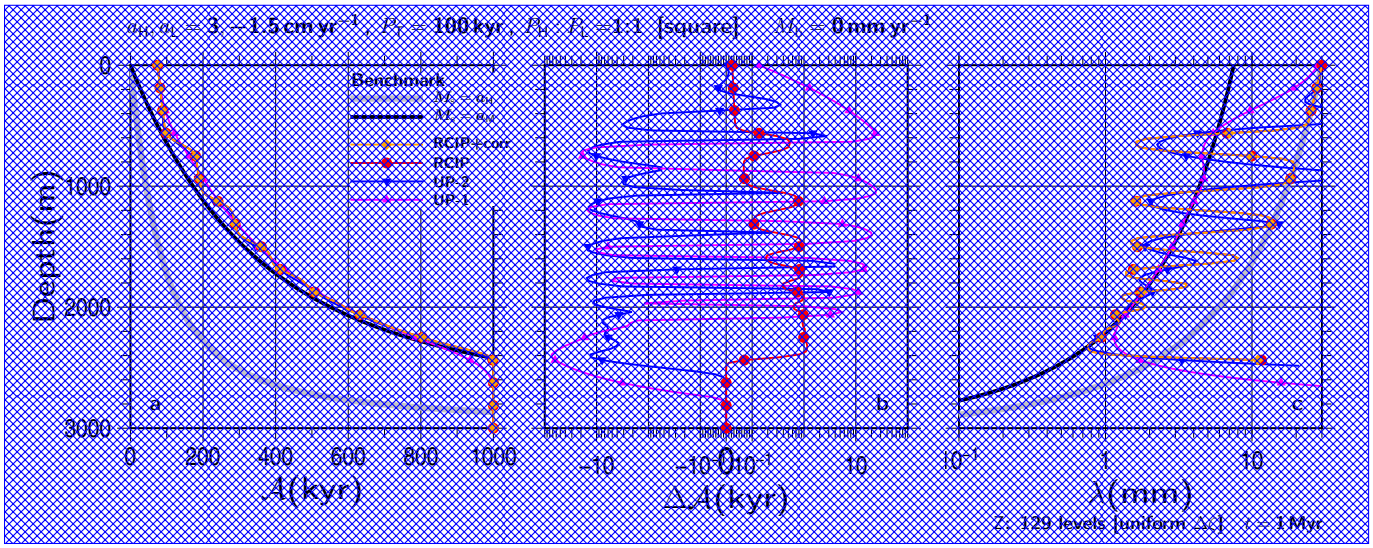

Figure ~~15. Same as Fig. 6, but for the results of transient experiments conducted using a square-wave surface mass balance with $a_L = -1.5\,\mathrm{cm\,yr^{-1}}$.~~ B3

Typically, in the experiments shown above, 100 kyr-cycle properties of input surface mass balance are maintained at around 300 to 500 kyr with the RCIP+corr(RCIP) scheme, and the computed age becomes smoother before that age (e.g., the square-wave shape in Fig. 10). The results obtained by UP-2 show loss of variation at similar or shallower depths, and those by UP-1 do so at even shallower depths, which results from the numerical diffusion of the schemes.

In the same manner as computing an approximate depth-age solution under constant surface/basal mass balance and constant thickness (e.g., the gray *benchmark* lines in Fig. 7a), the inverse age-depth solution can be also computed. Using this solution, 6
the vertical profiles of layers that are sufficient to hold a constant age difference ($\mathsf{T}_{\mathrm{res}}$) can be obtained. Figure 14b shows four 16
gray lines, which correspond to $\Delta\zeta$ sufficient to hold the 10, 5, 2, and 1 kyr differences when the experiment configuration is constant at $M_s = 1.5\,\mathrm{cm\,yr^{-1}}$, $M_b = 0$, and $H = 3000\,\mathrm{m}$. It is worth mentioning that for other M_s cases with the same M_b and H constant, the four reference ζ-$\Delta\zeta$ relationships correspond to those with $\mathsf{T}_{\mathrm{res}}$ divided by the factor of M_s for $M_s = 3\,\mathrm{cm\,yr^{-1}}$, and that they are interpreted as $\mathsf{T}_{\mathrm{res}} = 5$, 2.5, 1, and 0.5 kyr, respectively, while $M_s = 0.75\,\mathrm{cm\,yr^{-1}}$ are F
interpreted as $\mathsf{T}_{\mathrm{res}} = 20$, 10 4, and 2 kyr, respectively. Therefore, the $\Delta\zeta$ limit estimated by using the lower surface mass balance of the experiment should be considered. For example, if the grid size at a certain ζ is larger than the $\mathsf{T}_{\mathrm{res}} = 2\,\mathrm{kyr}$ line, characteristics with higher frequencies than $\mathsf{T}_{\mathrm{res}}$ cannot be sampled. The vertical line marked as Z: 129e in Fig. 14b corresponds 16
to uniform grid spacing of 129 levels adopted in the experiments conducted thus far. As the figure shows, this discretization can hold 2, 5, and 10 kyr differences by $\zeta \sim 0.82$, 0.44, and 0.29, respectively, and the 1 kyr is not resolved.

Figure 15 is the same as Fig. 7c, except for the results using the different P_T of 50, 20, and 10 kyr. As shown in the figure, 6
higher-frequency properties disappear at shallower depths. The results of RCIP(RCIP+corr) keep the oscillation relatively stable, but the computed annual layer thicknesses are not on the lines of the constant mass balance cases (gray lines), even at

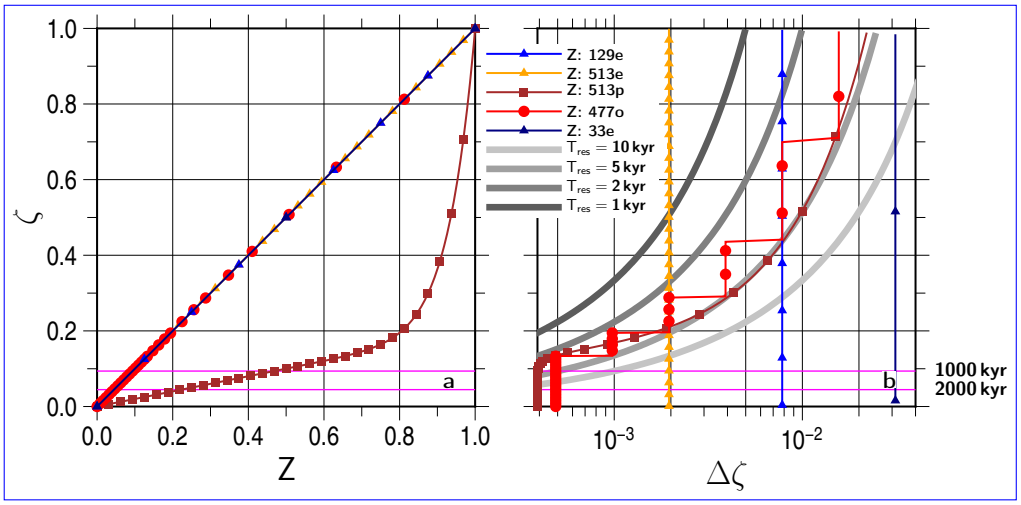

Figure 14 ~~16~~**.** Vertical discretization adopted in the present study: (a) Z vs ζ (b) $\Delta\zeta$ vs ζ. Five~~Four~~ patterns are shown: uniform grid spacing of 129 levels (129e), that of 513 levels (513e), a smooth non-uniform discretization (513p, see text), ~~and~~a non-smooth, non-uniform discretization (477o, see text), and uniform grid spacing of 33 levels (33e). Symbols are plotted for every 16 vertical levels. The four gray lines in (b) correspond to the layer thickness necessary to resolve 10, 5, 2, and 1 kyr differences under the condition of $M_s = 1.5\,\mathrm{cm\,yr^{-1}}$, $M_b = 0$, and $H = 3000\,\mathrm{m}$. The two horizontal magenta lines correspond to the depth needed to reach 1000 and 2000 kyr under the same conditions.

shallow depths, for high-frequency input (Fig. 15c). The square-wave shape pattern seems to be well preserved, at least around the 1700 m depth ($\zeta \sim 0.44$) in Fig. 15a, and around the 600 m depth ($\zeta \sim 0.8$) in Fig. 15b case (which is beyond the range of the figure but presented in the Supplement)~~Fig. 17b~~. Therefore, by~~in a~~ comparison with Fig. 14, it can be roughly estimated that $\mathsf{T}_{\mathsf{res}} = 5\,\mathrm{kyr}$ and $\mathsf{T}_{\mathsf{res}} = 2\,\mathrm{kyr}$ or longer are necessary to resolve the $P_{\mathsf{T}} = 50\,\mathrm{kyr}$ and $P_{\mathsf{T}} = 20\,\mathrm{kyr}$ square-wave shapes, respectively, which correspond to $1/10P_{\mathsf{T}}$.

Here, the same series of experiments is repeated using a higher resolution and a uniform grid spacing of 513 levels, which is four times the resolution of the previous experiments. The vertical line marked as Z: 519e in Fig. 14b corresponds to this grid spacing. As the figure shows, this discretization can hold 5, 2, and 1 kyr differences by $\zeta \sim 0.19$, 0.33, and 0.51, respectively, corresponding to 2430, 2010, and 1470 m in depth, respectively. The time step for higher resolution experiments conducted hereafter is set as 25 yr.

Figure 16 is the same as Fig. 15 except for the vertical grid spacing adopted and with zooming shown near the bottom part. The patterns seem to be well preserved by around the depths corresponding to the ζ above, but the computed ages produced by the RCIP+corr(RCIP) schemes are not on the line $M_s = a_L$ below the corresponding depths.

The number of vertical layers presented above exceeds 100, which is substantially more than those used in many operational large-scale 3D ice sheet models. The typical number of layers is 30, or even less (e.g., Goelzer et al., 2020; Seroussi et al., 2020). Therefore, since it would be helpful to evaluate performance levels at such a lower resolution for a broader range of

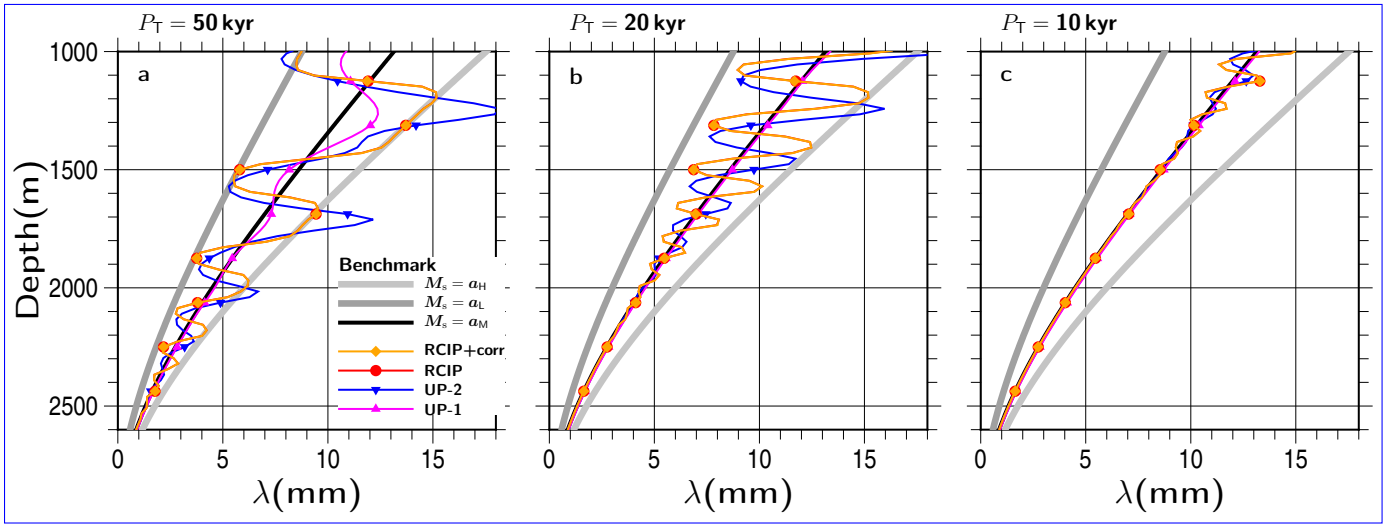

Figure 15 ~~17~~**.** Results of transient experiments conducted with the square-wave surface mass balances of $a_H, a_L = 3, 1.5\,\mathrm{cm\,yr^{-1}}$ and P_H : $P_L = 1:1$ (Eq. 57), and the total duration as (a) $P_T = 50\,\mathrm{kyr}$, (b) $P_T = 20\,\mathrm{kyr}$, and (c) $P_T = 10\,\mathrm{kyr}$~~(a) $P_T = 10\,\mathrm{kyr}$, (b) $P_T = 20\,\mathrm{kyr}$, and (c) $P_T = 50\,\mathrm{kyr}$~~. The basal mass balance is set as 0 for all the experiments in the figure. The vertical profiles of the annual layer thickness λ at $1000\,\mathrm{kyr}$ using RCIP+corr, RCIP (which overlaps with RCIP+corr), UP-2, and UP-1 are shown. The gray and black lines indicate benchmark solutions of constant surface mass balance cases with a_H, a_L, and $a_M = (a_H + a_L)/2$ given as references. Uniform grid spacing of 129 levels is adopted in this simulation. The results covering the depth from 1000 to 2600 m are shown. B020 B021

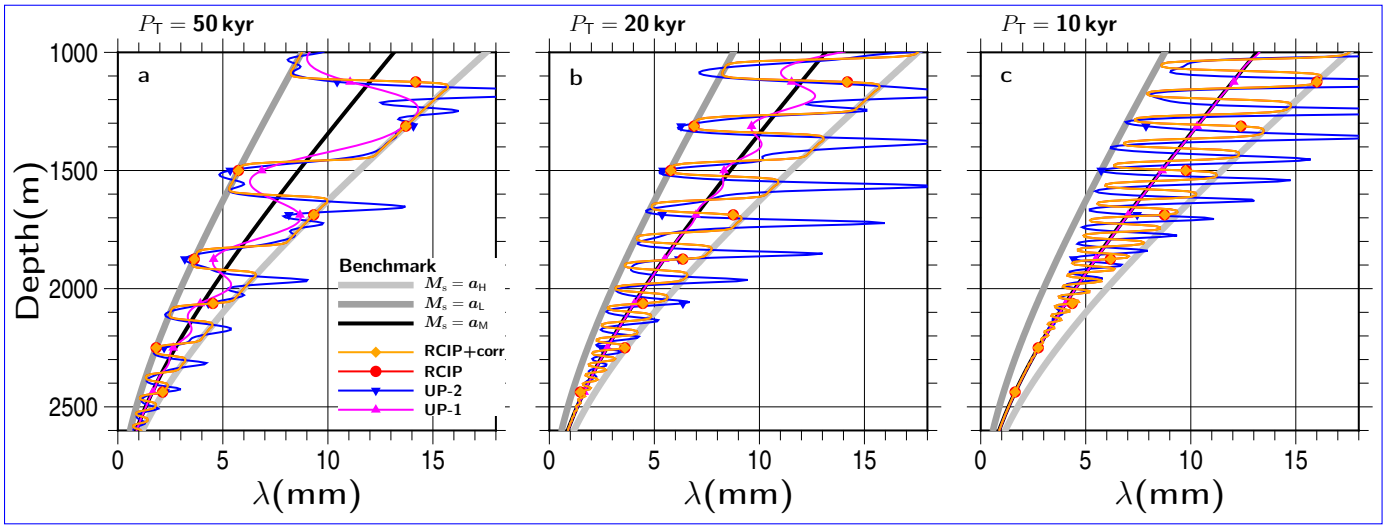

Figure 16 ~~18~~**.** Same as Fig. 15, except for the vertical resolution, which is shown as a uniform grid spacing of 513 levels. The results at 2000 kyr covering the depth from 1000~~1400~~ to 2600 m are shown. 17 B021

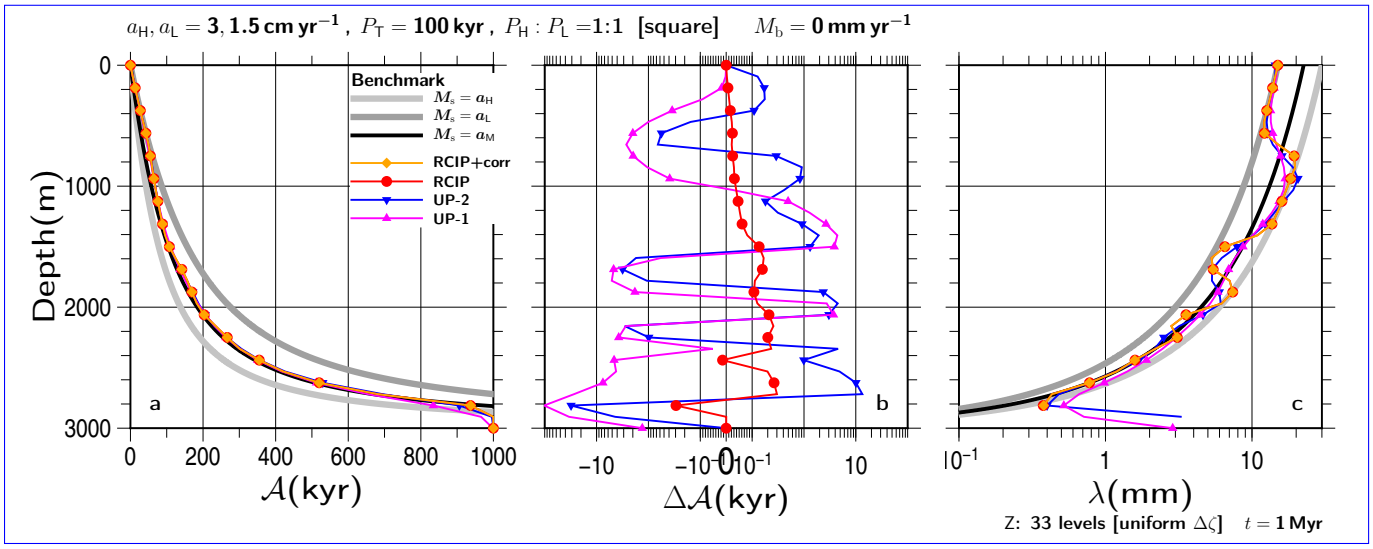

Figure 17. Same as Fig. 7, except for the experiment with the lower vertical resolution of 33 uniform grid spacing. Symbols are plotted for every two vertical levels.

applications, a series of experiments was performed using a lower resolution. Figure 17 is the same as Fig. 7, except that the results are provided using a uniform grid spacing of 33 levels (i.e., $\Delta z = 93.75\,\mathrm{m}$), which is one-fourth the resolution of the reference experiment. The time step for the lower resolution experiments was set to 200 yr.

When compared to the higher resolution cases, the annual layer thickness patterns seem to be less preserved. The square-wave pattern in the results of UP-1 has already disappeared at around 1400 m depth, while those in the other schemes are almost the same, although less than the 129-level cases.

Figure. 14b also contains a line corresponding to athe uniform grid spacing of 33 levels marked as Z: 33e. As the figure shows, this discretization can hold 10 kyr differences by $\zeta \sim 0.67$, corresponding to 990 m in depth. Similarly, it holdshold 20 kyr differences forby $\zeta \sim 0.43$, (1710 m, not shown in the figure). Figure 17c shows that the result patterns obtained for the RCIP+corr(RCIP) schemes are well preserved by around the 1400 m depth, which is between the two vertical levels of these estimations. Thus, likeThus as same as the 129-level cases, it can be roughly estimated that 1/10 (or slightly more) duration of the input cycle is necessary to resolve by one grid.

A comparison between Fig. 17b and Fig. 7b shows that differences in computed age among the schemes are within a comparable range ($\lesssim$ 10 kyr), and thus are neither exaggerated nor converged by reducing this resolution. The high-frequency oscillation seen near the bottom in Fig. 17b is not in Fig. 17b, which reflects the fact that even the RCIP+corr scheme cannot preserve the input shape near the bottom with the lower resolution. Nevertheless, it should be emphasized that there are still systematic 1 to 10 kyr biases are left by the upwind schemes.

3.8 Non-uniform discretization

So far, all of the experiments were performed with uniform discretization of either 129 or 513 levels. For most cases in the present study, it is reasonable to adopt non-uniform discretization, which means large spacing toward the top and small spacing toward the bottom. Since~~, in the previous section,~~ it was previously estimated that at least $1/10$ duration of the input cycle is necessary to resolve one grid, the discretization can be optimized according to the $\Delta\zeta$ profile computed with the minimum surface mass balance of the experiment. Here, for example, the target experiments are set as the square-wave surface mass balance with $P_\mathsf{T} = 100\,\mathrm{kyr}$, $P_\mathsf{H} : P_\mathsf{L} = 1:1$, $M_\mathrm{b} = 0$, $H = 3000\,\mathrm{m}$ constant, and $a_\mathsf{H}, a_\mathsf{L} = 3, 1.5\,\mathrm{cm\,yr^{-1}}$. This is the same configuration seen in Fig. 7. For this configuration, the combination of $\mathsf{T}_\mathsf{res} = P_\mathsf{T}/20 = 5\,\mathrm{kyr}$ and $M_\mathrm{s} = 1.5\,\mathrm{cm\,yr^{-1}}$ is adopted in order to compute the reference profile in the same way as Fig. 14. This number, which is half the number of the estimates used in the discussion above~~previous section~~, was chosen for safety, and to facilitate additional experiments with other configurations (e.g., $a_\mathsf{L} = 0.75\,\mathrm{cm\,yr^{-1}}$ and/or $P_\mathsf{T} = 50\,\mathrm{kyr}$, which are archived in the Supplement).

Two non-uniform discretization types are adopted in this section. One is a non-smooth grid, and the other is a smooth grid (introduced in Sect. 2.2). Various methods can be applied for non-smooth discretization. A very simple method, which is adopted in this study, calls for starting an initial spacing from the top and then keeping the same grid spacing as long as it is smaller than the reference profile. When the spacing exceeds the reference, it is halved from the coordinates and maintained at that size until it exceeds the reference again. It is necessary to limit the minimum grid spacing in order to avoid an infinite number of discretizations. The line marked as Z: 477o in Fig. 14 is a computed profile following the method mentioned above, which runs from $\Delta\zeta = 2^{-6}$ to 2^{-11}. It contains 477 levels from $\zeta = 0$ to $\zeta = 1$. The vertical coordinate system Z (model logical coordinate, see Sect.2.2) is identical to ζ, and the series of ζ_k is shown in Fig. 14a.

For non-uniform smooth discretization, a transformation function that follows the reference profile is necessary between ζ and Z. Since there is no fixed method for choosing the formulation of Z, the following three constraints are adopted for this paper: (i) $\zeta(\mathsf{Z}=0) = 0$, (ii) $\zeta(\mathsf{Z}=1) = 1$, and (iii) $\frac{\mathrm{d}\zeta}{\mathrm{d}\mathsf{Z}} > 0$ for $0 \le \mathsf{Z} \le 1$. A simple formulation to satisfy these constraints is

$$\zeta = \frac{\mathsf{Z} + \gamma \mathsf{Z}^\psi}{1+\gamma}, \tag{63}$$

where the two parameters γ (a weight) and ψ (a power) control the shape of transformation. The linear term Z in Eq. (63) is needed to avoid infinite $\frac{\partial \mathsf{Z}}{\partial \zeta}$ at $\zeta = \mathsf{Z} = 0$, which is used for in Eq. (45). After some trial and error with changing γ and ψ chosen from integer numbers, we found the following formulation can be used to maintain a grid spacing that is less than or equal to the reference profile until approaching the bottom: ~~After some trial and error, the following formulation was adopted:~~

$$\zeta \equiv \frac{\left(\mathsf{Z} + 4\mathsf{Z}^{14}\right)}{5}, \quad \mathsf{Z}_k = \frac{k}{\mathsf{N}_k - 1} \text{ for } k = 0, \cdots, \mathsf{N}_k - 1. \tag{64}$$

The line marked as Z:513p in Fig. 14 is the profile obtained by (64). ~~The linear term, Z/5, in Eq. (63) is needed to avoid infinite $\frac{\partial \mathsf{Z}}{\partial \zeta}$, which is used for in Eq. (45).~~Here, the same number of levels (513) is adopted to discretize under the Z-coordinate system. ~~The line marked as Z:513p in Fig. 16 is the profile obtained by (63), which maintains spacing smaller than or equal to the reference profile until near the bottom.~~Figure 14a shows the uniform grid spacing of Z, which corresponds to the non-uniform

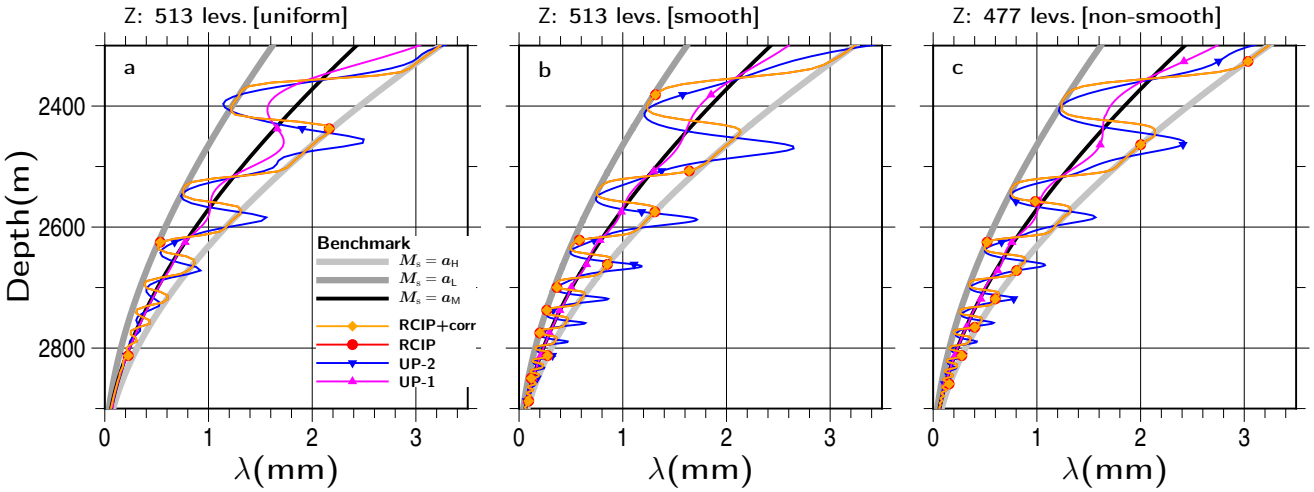

Figure 18 ~~19~~**.** Same as Fig. 7c, except for the vertical resolution as (a) uniform grid spacing of 513 levels, (b) smooth non-uniform grid spacing of 513 levels, and (c) non-smooth non-uniform grid spacing of 477 levels. The results at 2000 kyr covering the depths from 2300 to 2900 m are shown. 6

ζ grid spacing achieved by this method. Additionally, Fig. 14 marks the two vertical coordinates as references in order to reach 1000 and 2000 kyr, respectively, under the constant condition $M_s = 1.5\,\mathrm{cm\,yr^{-1}}$, $M_b = 0$, $H = 3000\,\mathrm{m}$. 16

Figures 18 and 19 show the results obtained using the uniform-spacing (Z:513e), smooth-grid (Z:513p), and non-smooth-grid (Z:477o) discretization methods, in terms of λ vs depth, and λ vs age. A comparison with Fig. 7 shows that the latter preserves the input shape deeper than the former. As shown in Fig. 14, the uniform discretization case (marked as Z:513e) is expected to fail to resolve 10 kyr at age 1000 kyr, which is presented in Fig. 19. The results of UP-1 preserved the input shape deeper than the lower resolution, which are almost only half of those achieved with the RCIP+corr(RCIP) methods. The results of UP-2 were preserved at slightly deeper depths than those of UP-1. However, their phases are shown to be shifted from those of the RCIP+corr(RCIP) methods, particularly at the deeper part. For differences in the computed age from the RCIP method (a and b), quantitatively, the same performance levels as the lower-resolution experiment were obtained by the other methods. The UP-1 and UP-2 methods deviate from the RCIP method by around 1 kyr and 10 kyr at most, while RCIP+corr deviates by around 100 yr. Using non-uniform discretization, preservation of the input shape is further extended to the deeper part (Fig. 18). As shown in Fig. 14, the non-smooth non-uniform discretization case (marked as Z:477o) crosses the $\mathsf{T}_{\mathsf{res}} = 10\,\mathrm{kyr}$ line at $\zeta \sim 0.07$ (i.e., 2790 m depth) for the $a_L = 1.5\mathrm{cm\,yr^{-1}}$ experiment, which is observed in Fig. 19. The smooth non-uniform discretization case (marked as Z:513p) crosses the $\mathsf{T}_{\mathsf{res}} = 10\,\mathrm{kyr}$ line slightly below that depth, $\zeta \sim 0.06$ (2820 m depth), which is observed in Fig. 19 again. In addition, similar to the lower-resolution experiment, Fig. 19 shows that the RCIP+corr(RCIP) scheme performs relatively better in terms of the phases than those with the UP-2 and UP-1 schemes. 20

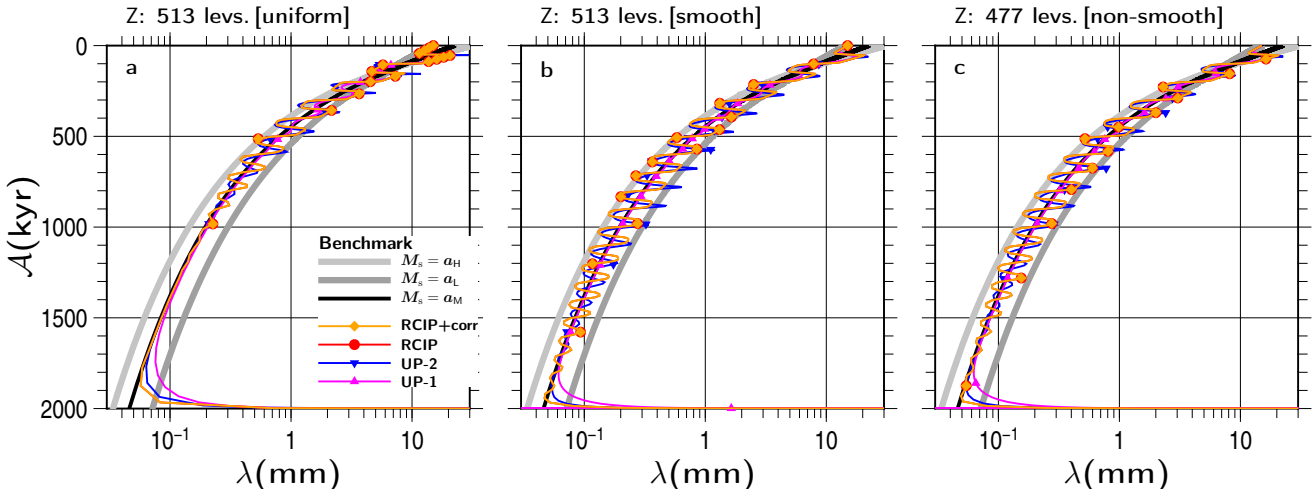

Figure 19 ~~20~~**.** Same as Fig. 10, except for the vertical resolution as (a) uniform grid spacing of 513 levels, (b) smooth non-uniform grid spacing of 513 levels, and (c) non-smooth non-uniform grid spacing of 477 levels. The results at 2000 kyr are shown.

4 Discussion and conclusion

The present study demonstrates a method for performing 1D age computations of ice-sheets under ~~various configurations, such as uniform velocity,~~constant velocity, variable velocity responding to transient changes in surface mass balance, and/or changes in ice-sheet thickness. Herein, comparisons~~Comparisons~~ of the vertical profiles of computed ages, as well as annual layer thicknesses, were~~are~~ examined among the RCIP schemes (semi-Lagrangian) and upwind schemes (Eulerian). Although the experiments in the present study were limited to 1D computations under summits, we believe the characteristics of the RCIP schemes have been presented sufficiently to allow evaluations of their performance levels. A008 A007

Overall, the RCIP schemes show the best performance levels among the schemes examined in the present study. In particular, the computed vertical profiles of the annual layer thicknesses produced by RCIP schemes follow the expected depth profiles more reasonably than the other methods. This advantage reflects the design of the RCIP scheme, which explicitly computes the evolution of the age derivative, i.e., the inverse of annual layer thickness, using an advection equation that is similar to the one used to compute the age itself. Using the other schemes, the computed vertical profiles of annual layer thickness either show more smoothing at shallower depths than that were found with the RCIP scheme or the development of oscillation at steep changes in the input surface mass balance. Such oscillation development is shown even when the input is a smooth cosine-wave type pattern and the amplitude is large. Since the slope filter adopted in this study is extremely simple, it is possible that the results obtained by the use of a second-order upwind scheme with a more suitable filter will change the characteristics. The introduction~~Introduction~~ of slope limiters on general non-uniform discretization for higher-order upwind schemes is possible (Murman et al., 2005), but the conditions used for switching between a cubic polynomial and a rational form (Eqs. 11 and 12) in the RCIP scheme may be simpler and easier to implement. Under some configurations, oscillation

development is not shown by the second-order upwind scheme. However, the phases of annual layer thickness against the age are shifted from those expected from the initial inputs, which again demonstrates the advantages of the RCIP scheme.

We examined two methods of computing the departure points in our RCIP scheme experiments. Under a constant velocity case, the results obtained by the simpler method show even less accurate solutions than the first-order upwind scheme, while the other 'correction' method shows the best performance. The computed age differences between the two RCIP methods is 1000 yr at most for all the configurations examined in the present study, including the vertical resolution. As a result, the simpler method still performs well if the expected accuracy of the application is less than that period. Under an evolving surface mass balance, the solution of the upwind schemes deviation is by 10 kyr, which is slightly larger.

As has already been discussed in previous studies(Greve et al., 2002), the first-order upwind scheme shows somewhat better performance than other schemes in some experiments. Greve et al. (2002) attributes this result to the cancellation of errors between discretization and numerical diffusion. In addition, from comparisons between results obtained via the first-order upwind scheme, with and without the mid-point rule, (Fig. 4), we find that the mid-point rule does provide an advantage 3 because the results obtained without the rule are worse by one order of magnitude than those obtained via the second-order upwind scheme. Furthermore, as discussed above, the upstream correction significantly improves the RCIP solution, which suggests that it is important to consider the non-constant velocity between the arrival and departure points. Since the mid-point rule formulation in the first-order scheme, in principle, corresponds to this upstream correction, they are consistent. The shape of the normalized vertical velocity profile also may play a role in the relative performance levels. For example, the upper part is more *linear* than the bottom part, which may increase the accuracy of the first-order approximation. In any case, it is clear that some or all of these points contribute to the higher performance of the first-order scheme, except for the bottom part.

As long as the annual layer thickness is not a concern, we feel that the classical upwind schemes are acceptable choices for use when dating. Note that using a first-order upwind scheme causes the structural details of the surface mass balance history to disappear very rapidly, but average features will compute quite well, except for near the bottom. The second-order scheme preserves the history better than the first-order scheme, but without an effective slope limiter, strange oscillations can appear in the results, as we have demonstrated in the present paper. However, in spite of these oscillations in the annual layer thickness, the results achieved by the second-order scheme are still slightly better than those for the first-order scheme throughout most of this study's experiments.

Greve et al. (2002) presented 'practical suggestions' for numerical dating schemes: the second-order, the total variation diminishing Lax-Friedrichs (TVDLF) scheme with the minimum modulus (min-mod) filter, and even the first-order upwind schemes. In line with those recommendations, we would like to add the following additional practical suggestions. If good performance is required from the annual layer thickness computation, we strongly recommend the application of RCIP. We also strongly recommend the application of RCIP if age computations near the bottom are required to be within the error range of, e.g., 10 kyr. In other cases, the classical upwind schemes are acceptable choices. B7

The ice thickness and accumulation rate values used in the present paper correspond to typical values found on the East Antarctic Plateau, and the values used for the cycles in surface mass balance are 10 to 100 kyr. Providing appropriate scaling is used, all of the results can be interpreted in the same way as those with different configurations. In order to simplify

the situation, the set of calculations will herein adopt a configuration with a different magnitude and surface mass balance cycle, while keeping the same thickness and zero mass balance. Figure 7 is taken as an example. In this experiment, we will use a figure with the same shape while replacing all the time related variables to $1/10$ — ten times higher accumulation rates ($a_{\mathrm{H}}, a_{\mathrm{L}} = 30, 15\,\mathrm{cm\,yr^{-1}}$) with $1/10$ cycles, $P_{\mathrm{T}} = 10\,\mathrm{kyr}$, $P_{\mathrm{H}}, P_{\mathrm{L}} = 5, 5\,\mathrm{kyr}$. The range of the horizontal axis needs to be adjusted from (a) $\mathcal{A}$ from 0 to $100\,\mathrm{kyr}$, (b) $\Delta\mathcal{A}$ from -1 to $1\,\mathrm{kyr}$, and (c) λ from 10^0 to $10^2\,\mathrm{mm}$, respectively (remember that the units of *annual* layer thickness λ are substantially $\mathrm{mm\,yr^{-1}}$). Similarly, Figure 15 can be interpreted as the results of (a) $P_{\mathrm{T}} = 5\,\mathrm{kyr}$, (b) $P_{\mathrm{T}} = 2\,\mathrm{kyr}$ and (c) $P_{\mathrm{T}} = 1\,\mathrm{kyr}$, respectively, providing that the horizontal axis is adjusted λ from 10^0 to $10^2\,\mathrm{mm}$. In summary, the results in the present paper can be interpreted as cases of $\sim 30\,\mathrm{cm/yr}$ surface mass balance with cycles of 1 to $10\,\mathrm{kyr}$, i.e., millennial-scale climate oscillations on a typical Greenland site. Under the scaled configuration, it can be interpreted from Fig. 7b that the age profiles produced by the RCIP scheme deviate from RCIP+corr by less than $100\,\mathrm{yr}$ throughout the depth range, which reflects the differences in computing the departure points. The other two schemes deviate by around $1\,\mathrm{kyr}$ at most. In addition, from Fig. 15a, it can be seen that the square-wave shape pattern is well preserved, at least around the $1700\,\mathrm{m}$ with $P_{\mathrm{T}} = 5$ (a) even though the higher-frequency properties disappear at shallower depths with $P_{\mathrm{T}} = 1\,\mathrm{kyr}$ case (c). Moreover, from examining a series of experiments with ten-times higher accumulation under $1/10$ shorter cycles, we confirmed the same normalized shape of the results (not shown). B4,B017

Although the focus of the present study is limited to 1D age computations, implementation of the RCIP scheme for 3D computation of the age field is also a suitable subject for future discussions. Extension to 3D would require the consideration of complex 3D flow fields and typically much lower horizontal ice age gradients. In addition, the negative mass balance experiment demonstrated in the present study is too simple to be compatible with the 3D situation. One important characteristic of the CIP scheme family is that the spatial gradient of the field variable (age in this case) is not a diagnostic (passive) value, but is instead a prognostic field. Yabe et al. (2002) argued that even in an extreme case where values of the three adjacent grid points are zero, one wave still can exist, and thus, non-zero spatial gradients can be held at these grid points. Therefore, it is speculated that the accuracy of the RCIP approach is not worse than that of other semi-Lagrangian schemes using higher-order interpolation techniques over the field variables, which have been discussed in past studies(Clarke and Marshall, 2002; Clarke et al., 2005). B5

As described in the present study, RCIP is an effective scheme for preserving the flux information at deposition (annual layer thickness in the case of dating). However, detection of 'points of origin' requires another technique, e.g., the back-tracing method. Huybrechts et al. (2007) suggested a very effective back-tracing method, which can be sufficient by itself for ice core dating. The small but primary advantage of the RCIP method over the powerful back-tracing method is that it is a forward scheme. This means that it is not necessary to record all the past velocity field data during the simulation. Therefore we consider the combination of the high-precision forward scheme and the powerful backward scheme to be a good choice when the objective is to obtain rough and detailed pictures of ice age fields. A1

Furthermore, it is expected that the RCIP scheme will be applicable to other advection problems in ice sheet modeling. The ~~In addition, the~~ evolutions of ice-sheet thickness and temperature are formulated using ~~the~~ transport or advection equations, A1 which are also good candidates for extending the discussion of this study. For such cases, researchers may be interested in mass

or energy conservation in the field. Actually, a multi-dimensional conservative formulation of CIP schemes has already been proposed (Yabe et al., 2002). Accordingly, the~~The~~ implementation of the scheme to 3D age and temperature fields in numerical ice-sheet models has already been set as the next target of our development.

Code availability. The copyright for the exact version of the model used in this study is held~~copyrighted~~ by Japan Agency for Marine-Earth Science and Technology (JAMSTEC) and~~which~~ is currently not publicly available. However, access~~Access~~ to the full code, including the scripts used to run the model for all the simulations presented in this paper, may~~an~~ be granted in response to requests tendered~~on demand by a request~~ to the corresponding author.

Appendix A: Notes on time-splitting

A time splitting technique (Eqs. 2 and 3) is at the~~a~~ core of the CIP schemes, and~~which~~ is somewhat difficult to understand at a first glance. We will attempt to clarify matters with the following simple explanation~~A simple explanation is tried as follows~~. If it is assumed that the non-advection term $h(x,t)$ satisfies at least locally $h(x,t) = h^*(t)$, i.e., is not dependent on x, a new variable $f^*(x,t)$ can be introduced such that

$$f^*(x,t) = f(x,t) - \int \mathrm{d}t\, h(x,t) \quad \simeq f(x,t) - \int \mathrm{d}t\, h^*(t)\,. \tag{A1}$$

Then, by introducing~~Introducing~~ Eq. (A1) into the original advection equation (1), a pure advection form of f^* can be obtained,

$$\frac{\partial f^*}{\partial t} + u(x,t)\frac{\partial f^*}{\partial x} = 0\,, \tag{A2}$$

which is the same form as~~to~~ the advection phase equation (2). Using a semi-Lagrangian algorithm, solving Eq. (A2) for f^* at time $t+\Delta t$ requires $f^*(x,t)$, which is identical to $f(x,t)$ by cancellation of the integral term of Eq. (A1). Therefore, Eq. (A2) is solved by the identical procedure used for~~of~~ Eq. (2). After solving $f^*(t+\Delta t)$, $f(t+\Delta t)$ can be computed using Eq. (A1), such that

$$f(x,t+\Delta t) = f^*(x,t+\Delta t) + \int_t^{t+\Delta t} \mathrm{d}t\, h^*(t)\,, \tag{A3}$$

which is the same as the non-advection equation (3) and the solution (21) where $f(x)$ is integrated with the initial condition f_j^*.

Appendix B: Implementation of RCIP method in the present paper

'Machine epsilon' is defined as the smallest ϵ in a computer such that $1+\epsilon > 1$ under floating-point arithmetic. Similarly, an arbitrarily number f has the corresponding smallest number (hereafter ε_f) which satisfies $f+\varepsilon_f > f$. In very rare cases, the

authors observed that the age at the upwind grid point becomes close to the value at the target grid point, which differs by ε_f (i.e., $f_{j+1} = f_j + \varepsilon_f$). Since no representative value exists between f_{j+1} and f_j under floating-point arithmetic, the upwind value is either f_j or f_{j+1}. Sometimes, f_{j+1} corresponds to a value at a grid point that is too far away to be transported. If there is an accumulation of errors of this type, the computed age may show unexpected oscillations.

Although rounding up very small differences may be a possible solution for such cases, a different approach was adopted in the present study. After some trials, ~~finally~~ the authors adopted finally the following procedure for avoiding such oscillations, which (to the degree they used it) worked better than the rounding-up procedure. In the numerical model of the present paper, Eq. (14) is transformed as follows:

$$F_j(X) = f_j + \frac{g_j X + C_2 X^2 + C_3 X^3}{1 + \alpha D_1 X} = f_j + \delta f \,, \tag{B1}$$

where C_1 and C_0 are substituted using Eqs. (18) and (19). The second term δf can be computed as the difference between f_j and f_{j+1}. When δf is non-zero but sufficiently small, i.e., less than ε_f, the value $f_j + \delta f$ is maintained as f_j. After simple reformulation, $F_j(X)$ in the model code is finally formulated as

$$F_j(X) = f_j + \frac{\hat{C}_1 X + \hat{C}_2 X^2 + \hat{C}_3 X^3}{\hat{D}_0 + \alpha \hat{D}_1 X} \,, \tag{B2}$$

where new series of constants are

$$\hat{D}_0 = |g_{j+1} - S_j| \,, \tag{B3}$$

$$\hat{D}_1 = D_1 \, |g_{j+1} - S_j| = \frac{|S_j - g_j| - |g_{j+1} - S_j|}{\Delta x_{j+\frac{1}{2}}} \,, \tag{B4}$$

$$\hat{C}_1 = g_j \, |g_{j+1} - S_j| \,, \tag{B5}$$

$$\hat{C}_2 = C_2 \, |g_{j+1} - S_j| = S_j \alpha \hat{D}_1 + \frac{(S_j - g_j) \, |g_{j+1} - S_j|}{\Delta x_{j+\frac{1}{2}}} - \hat{C}_3 \,, \tag{B6}$$

$$\hat{C}_3 = C_3 \, |g_{j+1} - S_j| = \frac{|g_{j+1} - S_j|}{\Delta x_{j+\frac{1}{2}}} \left[g_j - S_j + (g_{j+1} - S_j) + \alpha \hat{D}_1 \Delta x_{j+\frac{1}{2}} \right] \,, \tag{B7}$$

$$\tag{B8}$$

respectively. When $g_{j+1} - S_j = 0$ (and $\alpha = 1$), the coefficients lead to

$$\hat{C}_3 = 0, \quad \hat{C}_1 = 0, \quad \hat{D}_0 = 0 \,, \tag{B9}$$

$$\hat{C}_2 = S_j \frac{|S_j - g_j|}{\Delta x_{j+\frac{1}{2}}} \,, \tag{B10}$$

$$\hat{D}_1 = \frac{|S_j - g_j|}{\Delta x_{j+\frac{1}{2}}} \,, \tag{B11}$$

$$\tag{B12}$$

respectively, and using this combination, $F_j(X)$ is formulated as

$$F_j(X) = f_j + \frac{\hat{C}_2 X^2}{\hat{D}_1 X} = f_j + S_j X \,, \tag{B13}$$

which means a linear profile is adopted, regardless of g_j.

Author contributions. FS developed the ice-sheet model and then implemented the RCIP and other dating schemes ininto the model. FS performed numerical experiments designed by all the authors. The manuscript was written by FS with contributions from TO and AAO.

Competing interests. The authors declare that they have no conflicts of interest.

Acknowledgements. We would like to thank Shawn Marshall and an anonymous referee for their valuable comments, which have substantially improved our manuscript. This study was supported by the Japan Society for the Promotion of Science (JSPS) KAKENHI under Grant Numbers 17K05664, 17H06323, and 17H06104.

References

Clarke, G. K. and Marshall, S. J.: Isotopic balance of the Greenland Ice Sheet: modelled concentrations of water isotopes from 30,000 BP to present, Quaternary Science Reviews, 21, 419–430, https://doi.org/https://doi.org/10.1016/S0277-3791(01)00111-1, http://www.sciencedirect.com/science/article/pii/S0277379101001111, ePILOG, 2002.

Clarke, G. K. C., Lhomme, N., and Marshall, S. J.: Tracer transport in the Greenland ice sheet: three-dimensional isotopic stratigraphy, Quaternary Science Reviews, 24, 155–171, https://doi.org/10.1016/j.quascirev.2004.08.021, http://www.sciencedirect.com/science/article/B6VBC-4DS92J4-1/2/611027ceb4e1f74bb87ab3c501239d68, 2005.

Cuffey, K. M. and Paterson, W. S. B.: The Physics of Glaciers, Academic Press, fourth edn., 2010.

Fischer, H., Severinghaus, J., Brook, E., Wolff, E., Albert, M., Alemany, O., Arthern, R., Bentley, C., Blankenship, D., Chappellaz, J., Creyts, T., Dahl-Jensen, D., Dinn, M., Frezzotti, M., Fujita, S., Gallee, H., Hindmarsh, R., Hudspeth, D., Jugie, G., Kawamura, K., Lipenkov, V., Miller, H., Mulvaney, R., Parrenin, F., Pattyn, F., Ritz, C., Schwander, J., Steinhage, D., van Ommen, T., and Wilhelms, F.: Where to find 1.5 million yr old ice for the IPICS "Oldest-Ice" ice core, Climate of the Past, 9, 2489–2505, https://doi.org/10.5194/cp-9-2489-2013, http://www.clim-past.net/9/2489/2013/, 2013.

Goelzer, H., Nowicki, S., Payne, A., Larour, E., Seroussi, H., Lipscomb, W. H., Gregory, J., Abe-Ouchi, A., Shepherd, A., Simon, E., Agosta, C., Alexander, P., Aschwanden, A., Barthel, A., Calov, R., Chambers, C., Choi, Y., Cuzzone, J., Dumas, C., Edwards, T., Felikson, D., Fettweis, X., Golledge, N. R., Greve, R., Humbert, A., Huybrechts, P., Le clec'h, S., Lee, V., Leguy, G., Little, C., Lowry, D. P., Morlighem, M., Nias, I., Quiquet, A., Rückamp, M., Schlegel, N.-J., Slater, D., Smith, R., Straneo, F., Tarasov, L., van de Wal, R., and van den Broeke, M.: The future sea-level contribution of the Greenland ice sheet: a multi-model ensemble study of ISMIP6, The Cryosphere Discussions, 2020, 1–43, https://doi.org/10.5194/tc-2019-319, https://tc.copernicus.org/preprints/tc-2019-319/, 2020.

Greve, R. and Hutter, K.: Polythermal three-dimensional modelling of the Greenland ice sheet with varied geothermal heat flux, Annals of Glaciology, 21, 8–12, 1995.

Greve, R., Wang, Y., and Mügge, B.: Comparison of numerical schemes for the solution of the advective age equation in ice sheets, Annals of Glaciology, 35, 487–494, https://doi.org/10.3189/172756402781817112, 2002.

Huybrechts, P., Rybak, O., Pattyn, F., Ruth, U., and Steinhage, D.: Ice thinning, upstream advection, and non-climatic biases for the upper 89% of the EDML ice core from a nested model of the Antarctic ice sheet, Climate of the Past, 3, 577–589, https://doi.org/10.5194/cp-3-577-2007, https://www.clim-past.net/3/577/2007/, 2007.

Lhomme, N., Clarke, G. K. C., and Marshall, S. J.: Tracer transport in the Greenland Ice Sheet: constraints on ice cores and glacial history, Quaternary Science Reviews, 24, 173–194, https://doi.org/10.1016/j.quascirev.2004.08.020, http://www.sciencedirect.com/science/article/B6VBC-4DW2PC8-2/2/bff5252dbfb42af719bb6eeccb59bf05, 2005.

Mügge, B., Savvin, A., Calov, R., and Greve, R.: Numerical Age Computation of the Antarctic Ice Sheet for Dating Deep Ice Cores, in: Advances in Cold-Region Thermal Engineering and Sciences, edited by Hutter, Y. W. K. and Beer, H., pp. 307–318, Springer, 1999.

Murman, S., Berger, M., and Aftosmis, M.: Analysis of slope limiters on irregular grids, in: Technical Report NAS-05-007, NAS, 2005.

Parrenin, F., Dreyfus, G., Durand, G., Fujita, S., Gagliardini, O., Gillet, F., Jouzel, J., Kawamura, K., Lhomme, N., Masson-Delmotte, V., Ritz, C., Schwander, J., Shoji, H., Uemura, R., Watanabe, O., and Yoshida, N.: 1-D-ice flow modelling at EPICA Dome C and Dome Fuji, East Antarctica, Climate of the Past, 3, 243–259, 2007.

Rybak, O. and Huybrechts, P.: A comparison of Eulerian and Lagrangian methods for dating in numerical ice-sheet models, Annals of Glaciology, 37, 150–158, https://doi.org/10.3189/172756403781815393, 2003.

Seroussi, H., Nowicki, S., Payne, A. J., Goelzer, H., Lipscomb, W. H., Abe Ouchi, A., Agosta, C., Albrecht, T., Asay-Davis, X., Barthel, A., Calov, R., Cullather, R., Dumas, C., Gladstone, R., Golledge, N., Gregory, J. M., Greve, R., Hatterman, T., Hoffman, M. J., Humbert, A., Huybrechts, P., Jourdain, N. C., Kleiner, T., Larour, E., Leguy, G. R., Lowry, D. P., Little, C. M., Morlighem, M., Pattyn, F., Pelle, T., Price, S. F., Quiquet, A., Reese, R., Schlegel, N.-J., Shepherd, A., Simon, E., Smith, R. S., Straneo, F., Sun, S., Trusel, L. D., Van Breedam, J., van de Wal, R. S. W., Winkelmann, R., Zhao, C., Zhang, T., and Zwinger, T.: ISMIP6 Antarctica: a multi-model ensemble of the Antarctic ice sheet evolution over the 21st century, The Cryosphere Discussions, 2020, 1–54, https://doi.org/10.5194/tc-2019-324, https://tc.copernicus.org/preprints/tc-2019-324/, 2020.

Shashkov, M.: Conservative Finite-Difference Methods on General Grids, CRC press, Boca Raton, 1st edn., https://doi.org/10.1201/9781315140209, https://doi.org/10.1201/9781315140209, 1995.

Staniforth, A. and Côté, J.: Semi-Lagrangian Integration Schemes for Atmospheric Models: A Review, Monthly Weather Review, 119, 2206–2223, https://doi.org/10.1175/1520-0493(1991)119<2206:SLISFA>2.0.CO;2, https://doi.org/10.1175/1520-0493(1991)119<2206:SLISFA>2.0.CO;2, 1990.

Tarasov, L. and Peltier, W. R.: Greenland glacial history, borehole constraints, and Eemian extent, Journal of Geophysical Research, 108, 2143, https://doi.org/10.1029/2001JB001731, http://dx.doi.org/10.1029/2001JB001731, 2003.

Toda, K., Ogata, Y., and Yabe, T.: Multi-dimensional conservative semi-Lagrangian method of characteristics {CIP} for the shallow water equations, Journal of Computational Physics, 228, 4917–4944, https://doi.org/http://dx.doi.org/10.1016/j.jcp.2009.04.003, http://www.sciencedirect.com/science/article/pii/S0021999109001910, 2009.

Xiao, F., Yabe, T., and Ito, T.: Constructing oscillation preventing scheme for advection equation by rational function, Comp. Phys. Comm., 93, 1–12, https://doi.org/10.1016/0010-4655(95)00124-7, http://www.sciencedirect.com/science/article/pii/0010465595001247, 1996.

Yabe, T. and Takei, E.: A New Higher-Order Godunov Method for General Hyperbolic Equations, Journal of the Physical Society of Japan, 57, 2598–2601, https://doi.org/10.1143/JPSJ.57.2598, https://doi.org/10.1143/JPSJ.57.2598, 1988.

Yabe, T., Xiao, F., and Utsumi, T.: The Constrained Interpolation Profile Method for Multiphase Analysis, Journal of Computational Physics, 169, 556–593, https://doi.org/https://doi.org/10.1006/jcph.2000.6625, http://www.sciencedirect.com/science/article/pii/S0021999100966257, 2001.

Yabe, T., Ogata, Y., Takizawa, K., Kawai, T., Segawa, A., and Sakurai, K.: The next generation CIP as a conservative semi-Lagrangian solver for solid, liquid and gas, Journal of Computational and Applied Mathematics, 149, 267–277, https://doi.org/http://dx.doi.org/10.1016/S0377-0427(02)00535-6, http://www.sciencedirect.com/science/article/pii/S0377042702005356, scientific and Engineering Computations for the 21st Century - Methodologies and Applications Proceedings of the 15th Toyota Conference, 2002.